ACS APPLIED MATERIALS & INTERFACES

Research Article

www.acsami.org

Dendrimerlike Mesoporous Silica Nanoparticles as pH-Responsive Nanocontainers for Targeted Drug Delivery and Bioimaging

Liangliang Dai, Qingfeng Zhang, Jinghua Li, Xinkun Shen, Caiyun Mu, and Kaiyong Cai*

Key Laboratory of Biorheological Science and Technology, Ministry of Education College of Bioengineering, Chongqing University, Chongqing 400044, P. R. China

Supporting Information

ABSTRACT: In this work, we employed dendrimerlike mesoporous silica nanoparticles with hierarchical pores (HPSNs) to fabricate drug delivery system bioimaging and targeted tumor therapy in vivo. *N*,*N*-phenylenebis-(salicylideneimine)dicarboxylic acid (Salphdc) was used both as the gatekeeper of HPSNs via pH-responsive coordination bonds between −COOH of Salphdc and In^{3+} ions and as a fluorescence imaging agent. Folic acid was then conjugated to Salphdc as the targeting unit. The results revealed that the system could deliver model drug DOX to the tumor site with high efficiency and then cause cell apoptosis and tumor growth inhibition. Moreover, the conjugated Salphdc was proved to be a promising fluorescence probe for tracing distribution of the system in vivo. The study affords a potential nanoconainer for cancer therapy and biological imaging.

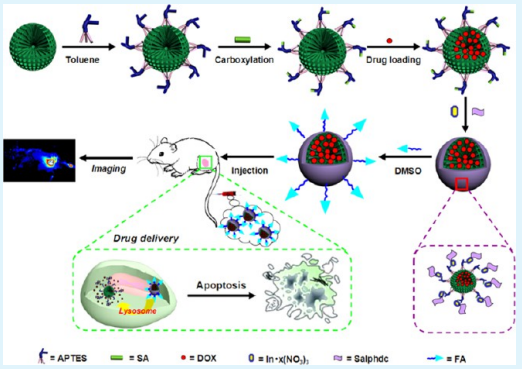

KEYWORDS: *dendrimerlike silica nanoparticles, pH-response, targeted drug delivery, in vivo, bioimaging*

INTRODUCTION

In recent years, diverse carriers were developed to achieve desired drug delivery performances. For instance, dendrimer, a branched macromolecule, has been exploited to be a potential carrier for drug delivery, due to its unique nanoscale morphology, large surface area, and good monodispersity. Nevertheless, one type of dendrimer has only a single type of termini. Moreover, its controlled release kinetics is difficult to handle.[1,2] Furthermore, its multifunctionalization remains tedious and challenging.[3] In contrast, mesoporous silica nanoparticles (MSNs) are easy to modify with various functional components for the fabrication of a multifunctional drug delivery system. They demonstrated multifunctions both as controlled drug release vehicles and imaging probes.[4,5] Moreover, the loading drugs could be released in response to diverse stimuli including pH,[6,7] enzymes,[8,9] temperature,[10] light,[11] redox,[12−14] etc. Therefore, silica nanoparticles with hierarchical pores (HPSNs) attracted much attention due to their similar morphology to organic dendrimer and silica physicochemical properties including good biocompatibility, large surface area, high stability, and easy surface functionalization.[15−17]

As for MSNs-based controlled release systems, various physicochemical signals deriving from the tumor microenvironment were employed as stimuli for triggering drug delivery, in particular of pH signal.[6,7] The potential inflammatory reaction and overconsuming of oxygen by tumor cells results in an acidic tumor microenvironment. Moreover, the formed endosomes and/or lysosomes after cell uptake of drug delivery systems are also acidic.[18] Diverse strategies have been developed to control drug release via pH signal. To date, there are mainly five types of strategies, including dissolution of pore-blocking agents,[19,20] reduction of charge interaction,[21,22] transformation between hydrophilicity and hydrophobicity,[18,23] conformational change,[24] and bond breakage.[25,26] As for pH-responsive MSNs drug delivery systems, inorganic nanoparticles, such as gold nanoparticles[25] and Fe_3O_4,[27] were used as gatekeepers to seal the mesopores of MSNs, mainly due to their high blocking efficiency. However, the subsequent clearance of inorganic nanoparticles from a host is a potential challenge, which limits their clinical application. In contrast, to employ biocompatible macromolecules and/or polymer as gatekeepers of MSNs displayed great advantages, such as improving the biocompatibility of MSNs, stabilizing the drug delivery system, facilitating conjugation of targeting moieties, prolonging blood circulation lifetimes, etc.[28,29] Previously, we developed different MSN-based drug delivery systems with improved biocompatibility by using natural macromolecules such as heparin, collagen, gelatin, etc., as gatekeepers.[6,12,30] Thus, grafting a macromolecules/polymer onto the surface of HPSNs via an acid cleavable linker is a promising approach for construction of pH-responsive delivery systems which has great potential for clinical applications. Nevertheless, few studies have been reported related work.[15,31]

With the advancement of nanotechnology, developing imaging-guided multifunctional drug delivery systems has attracted much attention either for fundamental research or

Received: January 25, 2015
Accepted: March 12, 2015
Published: March 12, 2015

DOI: 10.1021/acsami.5b00746
ACS Appl. Mater. Interfaces 2015, 7, 7357−7372

potential clinical applications,[21,32] since real-time imaging would provide great convenience for diagnosis and therapy. In detail, imaging-guided multifunctional drug delivery systems could be easily visualized at a specific site during its metabolic pathways and then trigger the drug delivery by external stimuli, to maximize the efficiency of therapeutic agents. Fluorescent dyes and quantum dots have been widely used as imaging agents in related fields.[33−35] A previous study reported that *N*,*N*-phenylenebis(salicylideneimine)dicarboxylic acid (Salphdc) had a unique autofluorescence feature with good biocompatibility.[36] It could easily interact with metal ions to form metal−organic framework thin films.[37,38] Thus, it provides convenience by employing Salphdc to construct an imaging-guided drug delivery system.

Moreover, as for clinical application, the potential side effects of a drug delivery system should be considered. To achieve targeted intracellular drug delivery is one way to reduce its toxic side effects for cancer therapy. Previously, many molecules were exploited to be targeting motifs anchoring to drug delivery systems for cancer therapy, such as lactobionic acid (LA),[12,30,39] peptide,[40,41] folic acid (FA),[13,42] etc. FA, as a common targeting motif, anchors to the tumor site via receptor−ligand recognition. Generally, around 40% of human tumors overexpress folate receptors, whereas healthy cells have no folate receptor expression.[43] Thus, FA was selected as a targeting component in the system.

Recently, we fabricated a redox-responsive system for controlled drug release with MSNs for tumor-targeted therapy, by using heparin as the gatekeeper and LA as the targeting component.[12] In the present study, we developed a pH-responsive drug delivery system with HPSNs as the nanocontainer, Salphdc complex as the gatekeeper, and FA as the targeting unit, respectively. Moreover, the system could be employed for bioimaging due to the gatekeeper Salphdc complex. The rationale for choosing the HPSN as a nanocontainer lies in the following: first, an HPSN has unique mesoprous characteristics, i.e. gradually decreasing pore sizes from the surface to center of particles for facilitation of easy drug loading when compared with an MSN; second, HPSNs share desirable physicochemical properties of MSNs. The fabrication of the controlled drug release system was presented as follows (Scheme 1): First, we synthesized HPSN and modified them by using amino and carboxyl groups. Next, Salphdc and $In(NO_3)_3{\cdot}xH_2O$ were added to the dimethylformamide (DMF) solution containing HPSN−COOH, and the complexation reaction between −COOH of Salphdc and In^{3+} ions was allowed to proceed. Then the formed coordination macromolecules were deposited onto the HPSN−COOH, leading to the gradual evolution of the Salphdc shell that was sensitive to acid. The formed Salphdc shell not only sealed the hierarchical pores of the HPSN but also would be used for bioimaging in vivo. Finally, FA grafted to Salphdc end-capping the HPSN for the targeting of tumor cells. Therefore, we hypothesized that the multifunctional HPSN was a potential pH-responsive vehicle for targeted drug delivery, with fluorescent imaging potential.

RESULTS AND DISCUSSION

HPSNs were synthesized with an ethyl ether emulsion approach as previously reported.[44] The transmission electron microscopy (TEM) and scanning electron microscopy (SEM) were employed to characterize the nanoparticles. The synthesized HPSNs exhibited hierarchical pore structure on the surface (Figure 1A, Figure S1), and the multifunctionalized nanoparticles (HPSN−Salphdc−FA) displayed similar morphology to that of HPSNs. Nevertheless, an obvious shell layer adhered to the HPSN surface was observed in TEM images (Figure 1B, Figure S1). The average sizes of HPSNs and HPSN−Salphdc−FA were 106 ± 11 and 117 ± 13 nm (Figure S2), respectively, which was revealed by dynamic light scattering (DLS) measurement. The phenomenon could be explained that SA, Salphdc, FA molecules, etc., were covalently conjugated to the surfaces of HPSNs, resulting in the increase of the diameters and changing of morphology of HPSN−Salphdc−FA. And the significant difference between the inside and shell of HPSN−Salphdc−FA also suggested that Salphdc and FA molecules were successfully coupled to HPSNs.

Next, thermogravimetric analysis (TGA) was used to characterize the process of surface functionalization of HPSNs. The TGA curves of loss weight demonstrated that Salphdc and FA molecules were conjugated to HPSNs. Moreover, the model dug of DOX was successfully loaded into HPSN−Salphdc−FA (Figure 1C), with an encapsulation content of around 4.87 wt %.

Furthermore, we quantitatively measured encapsulation efficiency and loading degree of the system. The loading degree and encapsulation efficiency of HPSN−Salphdc−FA were determined as 4.92 wt % and 37.44%, respectively. The data of loading degree was consistent with that of TGA.

To systematically reveal the successful introduction of the above molecules to HPSNs, various techniques were employed to characterize the samples. Brunauer−Emmett−Teller (BET) measurement revealed that HPSNs displayed a type-IV isotherm curve, with surface area of 862 m^2/g. The result indicates the mesoporous structures of HPSNs.[45] Then, the surface areas of HPSN−COOH and HPSN−Salphdc−FA decreased to 548 and 58 m^2/g, respectively. Barrett−Joyner−Halenda (BJH) analysis proved that the pore sizes decreased accordingly as well (Figure S3 and Table S1). These results also suggested that Salphdc and FA molecules were indeed coated onto HPSN and blocked the mesopores of HPSN. Besides, Fourier transform infrared spectroscopy (FTIR) spectra and ^1H NMR spectra indicated that HPSN−Salphdc−FA was successfully constructed after multimodifications (Figure S4 and S5). Furthermore, the ^1H NMR spectra confirmed that the conjugation efficiency of FA was 27.4%. The zeta potential of the nanoparticles changed with each modification (Table S2), indicating that −COOH group, Salphdc, and FA were conjugated onto the surface of HPSNs. For instance, compared with that of HPSNs, the zeta potential of HPSN−COOH shifted from −2.37 to −24.3 mV, which was attributed to the introduction of SA molecules. All results suggest that HPSN−Salphdc−FA was successfully fabricated.

We employed UV/vis/NIR spectrum analysis to reveal the drug release behavior of the DOX@HPSN−Salphdc−FA system. PBS buffer with various pH values was used as external stimuli. At physiological pH, only a little amount of DOX was leaked from DOX@HPSN−Salphdc−FA after incubation for 24 h, due to the end-capping with Salphdc. The result suggests that the system had relatively good sealing efficiency. However, when the HPSN−Salphdc−FA system was exposed to PBS buffer (pH 5.0), obvious DOX release from DOX@HPSN−Salphdc−FA was observed (Figure 2A). For long-term drug release of the HPSN−Salphdc−FA system, the result demonstrated around 60% of DOX was released from the system when exposing it to PBS with pH 5.0 for 60 h. In contrast, only around 10% of DOX was released from the system under pH of

DOI: 10.1021/acsami.5b00746
ACS Appl. Mater. Interfaces 2015, 7, 7357−7372

Scheme 1. Construction of pH-Responsive HPSN−Salphdc−FA System: (A) Chemical Reaction Routes and (B) Drug-Loaded HPSN−Salphdc−FA System for Tumor Therapy and Bioimaging in Vivo

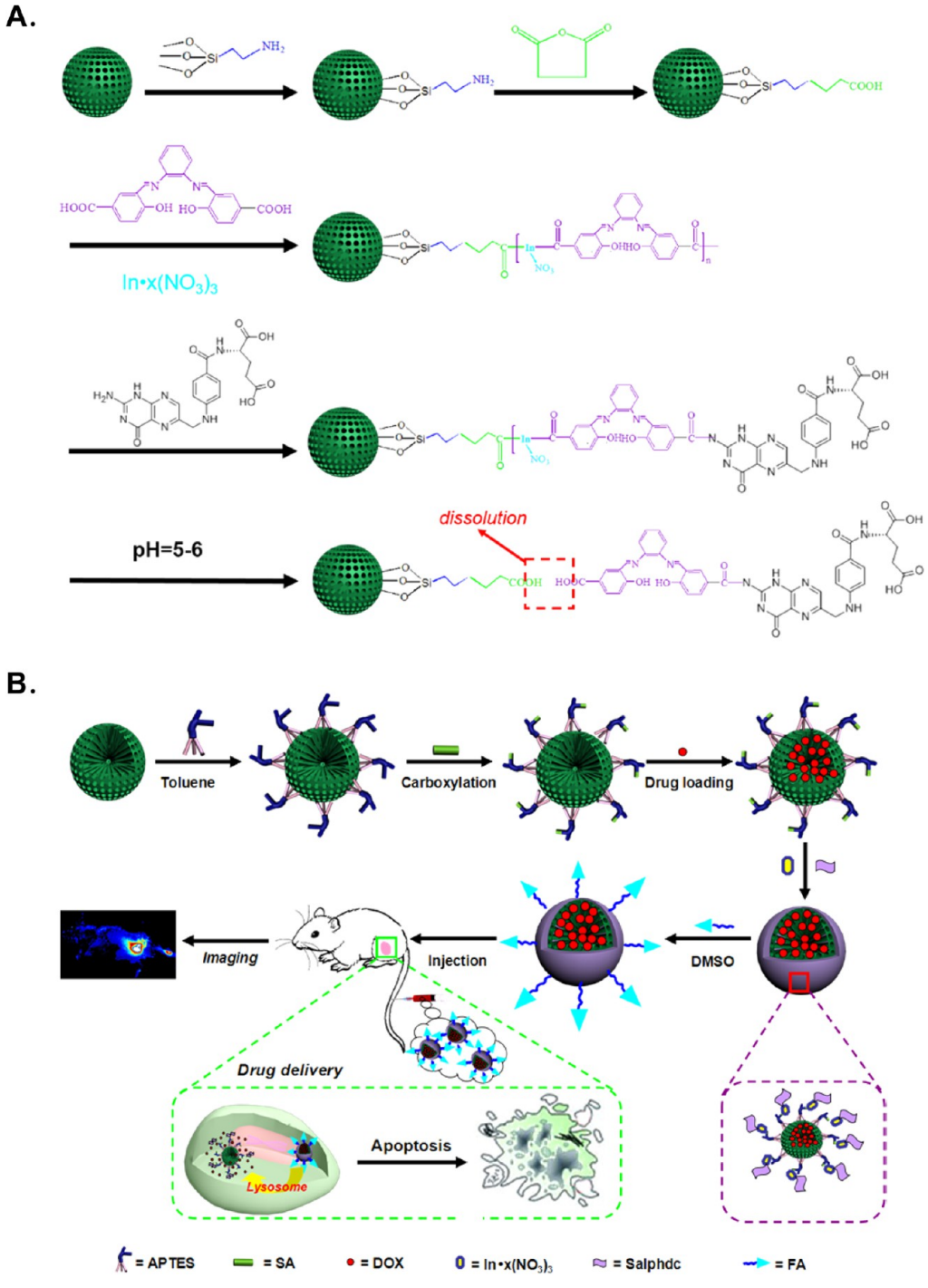

7.4 for 60 h (Figure 2B). The phenomenon could be interpreted as dissolution of the Salphdc coordination polymers under an acidic environment, exposing the inherent mesopous access on the surfaces of HPSNs, resulting in quick DOX release from the system. Considering the acidic environment of tumor and inflammatory tissues, and the lower pH value of endosomes and/or lysosomes, the results imply that the HPSN−Salphdc−FA system is suitable for tumor therapy.

To evaluate the biocompatibility of the HPSN−Salphdc−FA system, we performed a CCK8 assay in this study. The cell viability of three groups was no different when HepG2 cells were incubated with tissue culture polystyrene plate (TCPS, control) and cocultured with HPSNs and HPSN−Salphdc−FA for 6, 12, 24, and 48 h, respectively. Meanwhile, the cell viability of the HPSN−Salphdc−FA group was observed to be slightly higher than the HPSN group in all time periods (Figure 3A), indicating that HPSN−Salphdc−FA was of good biocompatibility.

Next, the dose-dependent cytotoxicity assay of DOX@HPSN−Salphdc−FA was investigated to further evaluate the biocompatibility. At low concentration of DOX (from 0.3125 to 0.625 μg/mL), the viability of HepG2 cells was no different from the control, upon treatment with DOX@HPSN−Salphdc−FA

DOI: 10.1021/acsami.5b00746
ACS Appl. Mater. Interfaces 2015, 7, 7357−7372

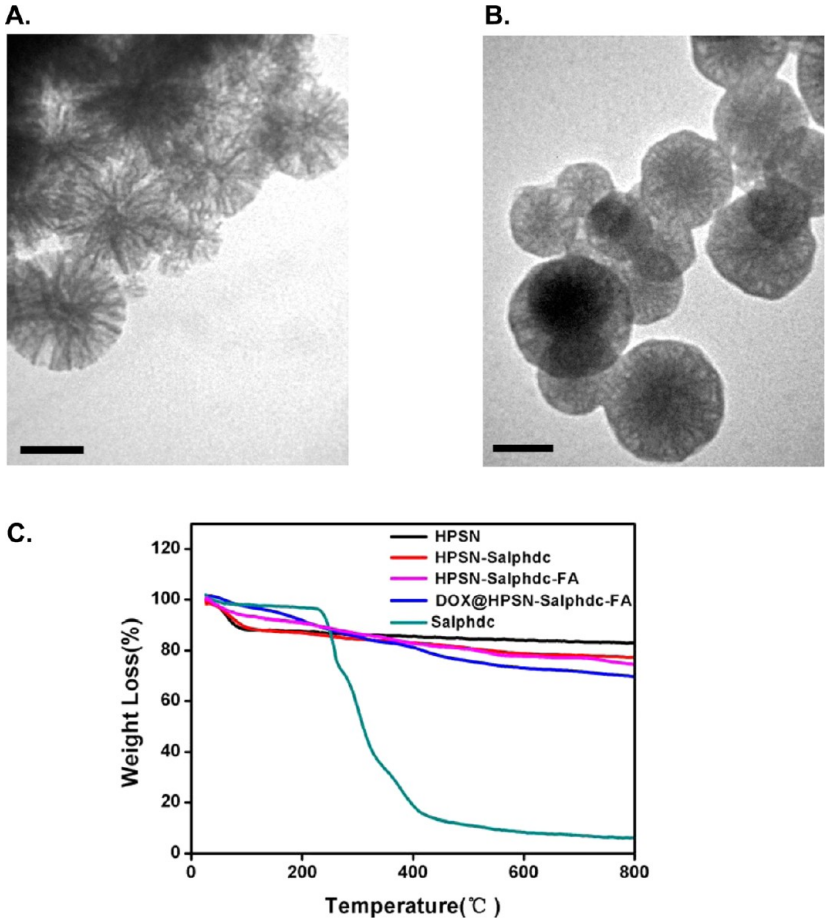

Figure 1. Physical properties of different HPSN nanoparticles: TEM pictures of (A) HPSNs and (B) HPSN−Salphdc−FA and (C) TGA curves of HPSNs, Salphdc, HPSN−Salphdc, HPSN−Salphdc−FA, and DOX@HPSN−Salphdc−FA, respectively. The scale bar is 50 nm.

for 48 h. While at high concentration of DOX (from 1.25 to 10 μg/mL), DOX@HPSN−Salphdc−FA treated cells revealed significantly lower ($p < 0.01$) cell viability than free DOX in each concentration group. In contrast, when HepG2 cells were cocultured with DOX@HPSN−Salphdc−FA at high concentration (equivalent of 10 μg/mL DOX) for 48 h, the cell viability sharply reduced to around 12% (Figure 3B). The cytotoxic effect of DOX@HPSN−Salphdc−FA could be interpreted as the low pH of endosome/lysosome triggering DOX release after DOX@HPSN−Salphdc−FA was endocytosed by HepG2 cells, thus high local concentration of DOX was accumulated in HepG2 cells and induced cell apoptosis. Moreover, the previous study reports similar result about the dose-dependent cytotoxicity assay of MSNs.[12,46] The results imply that the DOX@HPSN−Salphdc−FA system might be a promising drug release platform for in vivo tumor treatment.

Subsequently, we used TEM to explore the distributions of HPSNs and HPSN−Salphdc−FA after endocytosis in vitro. After the HepG2 cells were incubated with HPSNs and HPSN−Salphdc for 6, 12, and 24 h and HL-7702 cells were cocultured with the above nanoparticles for 24 h, respectively, it was observed that both cell membranes were intact and nuclei were distinct as well owing to the good biocompatibility of these nanoparticles. The result was in accordance with the biocompatibility assessment (Figure 3A). It was also observed that the endocytosed nanoparticles entered the cytoplasm rather than the nuclei, which was supported by previous reports.[47,48] Furthermore, the dispersion morphology of HPSN−Salphdc−FA was shown to be better than that of HPSNs within both cells (Figure 4A, dash frame, and Figure S6). Obviously, a higher amount of HPSN−Salphdc−FA was taken up by HepG2 cells (Figure 4A, b vs a) vs HPSNs. As for negative control, the number of endocytosed HPSN−Salphdc−FA nanoparticles by HL-7702 cells was similar to that of HPSNs, mainly due to the fact that HL-7702 cells only expressed little FA receptor.[49] Nevertheless, after culture for 24 h, HepG2 cells took up higher amounts of either HPSN−Salphdc−FA or HPSNs than those HL-7702 cells. The phenomenon could be attributed to two factors: first, the metabolism of HepG2 cells is higher than that of HL-7702 cells; second, HepG2 cells overexpressed FA receptor, thus mediating cellular uptake.

Then, confocal laser scanning microscopy (CLSM) was employed to observe and analyze the distribution of nanoparticles within HepG2 cells quantitatively (Figure 4B). Both endocytosed HPSN−Salphdc and HPSN−Salphdc−FA were observed at the entrance to cytoplasm after incubation for 6, 12, and 24 h. With the increasing incubation time, the number of endocytosed HPSN−Salphdc and HPSN−Salphdc−FA obviously increased. CLSM images displayed the process of cell endocytosis (Figure 4B, arrows). Moreover, the amount of HPSN−Salphdc−FA taken up was significantly higher than the HPSN group at all times ($p < 0.01$, Figure 4C and D), indicating that FA receptor being overexpressed by HepG2 cells improved the cell endocytosis.[13] It thus led to HepG2 cells taking up more HPSN−Salphdc−FA.

DOI: 10.1021/acsami.5b00746
ACS Appl. Mater. Interfaces 2015, 7, 7357−7372

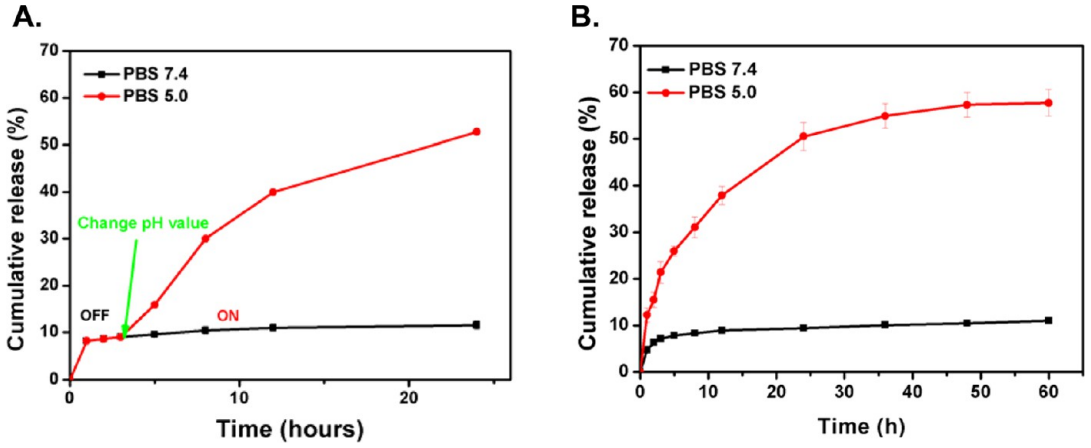

Figure 2. (A) Release behavior of the control (pH 7.4) and pH-stimuli groups (pH 5.0). The pH value was changed in the system after incubation for 3 h (arrow). (B) pH-Responsive release behavior of DOX from the system under pH values of 7.4 and 5.0 over 60 h.

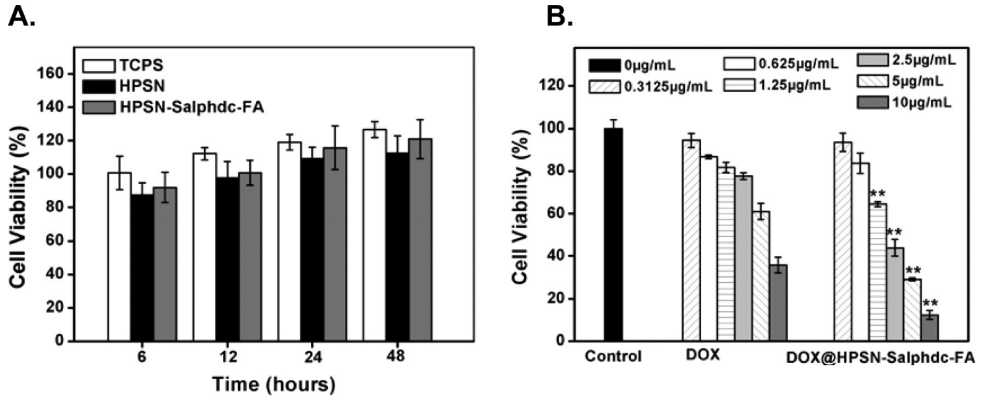

Figure 3. (A) Cytotoxicity assay of HPSNs and HPSN−Salphdc−FA (0.4 mg/mL) with HepG2 cells as compared with the control group (TCPS). (B) Normalized viability of HepG2 cells when cocultured with free DOX and DOX@HPSN−Salphdc−FA with different concentrations for 48 h. The error bars reflect mean ± SD (n = 6), (**) $p < 0.01$.

Furthermore, HepG2 cells were incubated with nanoparticles at different conditions to reveal the cell endocytosis mechanism of different HPSN nanoparticles. First, energy-dependent endocytosis pathway was investigated by treating the cells with sodium azide and 4 °C, resulting in significant decrease of cell uptake efficiency (Figure 4E, left). The reason was that sodium azide could block the synthesis process of adenosine 5-triphosphate (ATP), and 4 °C could inhibit the energy metabolism in the cells.[50] It indicates that the energy is essential for endocytosis of HPSN−Salphdc and HPSN−Salphdc−FA. The result was supported by a previous study.[6] Second, other types of endocytosis pathways were investigated by treating the cells with genistein, amiloride−HCl and amantadine−HCl, respectively. Genistein could inhibit caveolae-mediated cell uptake.[51] The result suggests a little effect on the endocytosis of HPSN−Salphdc−FA and HPSN−Salphdc. Amiloride−HCl could inhibit micropinocytosis-mediated cell uptake,[52] which caused around 89% and 93% decrease in endocytosis efficiency of HPSN−Salphdc−FA and HPSN−Salphdc, respectively. While amantadine−HCl could block clathrin-mediated cell uptake, which obviously reduced the cell endocytosis of both HPSN−Salphdc and HPSN−Salphdc−FA (Figure 4E, right). The results demonstrate that cell uptakes of HPSN−Salphdc and HPSN−Salphdc−FA were mainly mediated via macropinocytosis- and clathrin-mediated endocytosis pathways. HPSN−Salphdc−FA was more probably to be uptaken by cells via clathrin-mediated endocytosis pathway, in comparison to that of HPSN−Salphdc through macropinocytosis. The result could be explained that HPSN−Salphdc was physically attached to cytomembrane and then endocytosed via macropincytosis pathway.[53] Furthermore, HPSN−Salphdc−FA was uptaken via clathrin-mediated endocytosis, which was contributed to the receptor-mediated endocytosis deriving from FA molecules.[54]

To further demonstrate FA receptor-mediated endocytosis of HPSN−Salphdc−FA nanoparticles, HepG2 cells was cultured with FA to block the receptors on the cell membranes before treated with HPSN−Salphdc−FA.[42] CLSM was utilized to visualized HPSN−Salphdc−FA endocytosed by HepG2 cells. The uptaken HPSN−Salphdc−FA nanoparticles by HepG2 cells were obviously distributed in the cytoplasm of cells. When HepG2 cells were pretreated with FA, the amount of uptaken nanoparticles by HepG2 was significantly decrease ($p < 0.01$), in corresponding with the quantification analysis of fluorescence intensity (Figure 5A and B). The results prove that FA receptor-mediated endocytosis mainly contributed to the HepG2 cells' uptake of HPSN−Salphdc−FA nanoparticles. Moreover, to reveal the cell specific endocytosis of HPSN−Salphdc−FA by HepG2 cells, we used human umbilical vein endothelial cells (HUVEC) as control in this study. Flow cytometry (FCM) analysis was performed. It turned out that the endocytosis level for HPSN−Salphdc−FA by HUVEC cells

DOI: 10.1021/acsami.5b00746
ACS Appl. Mater. Interfaces 2015, 7, 7357−7372

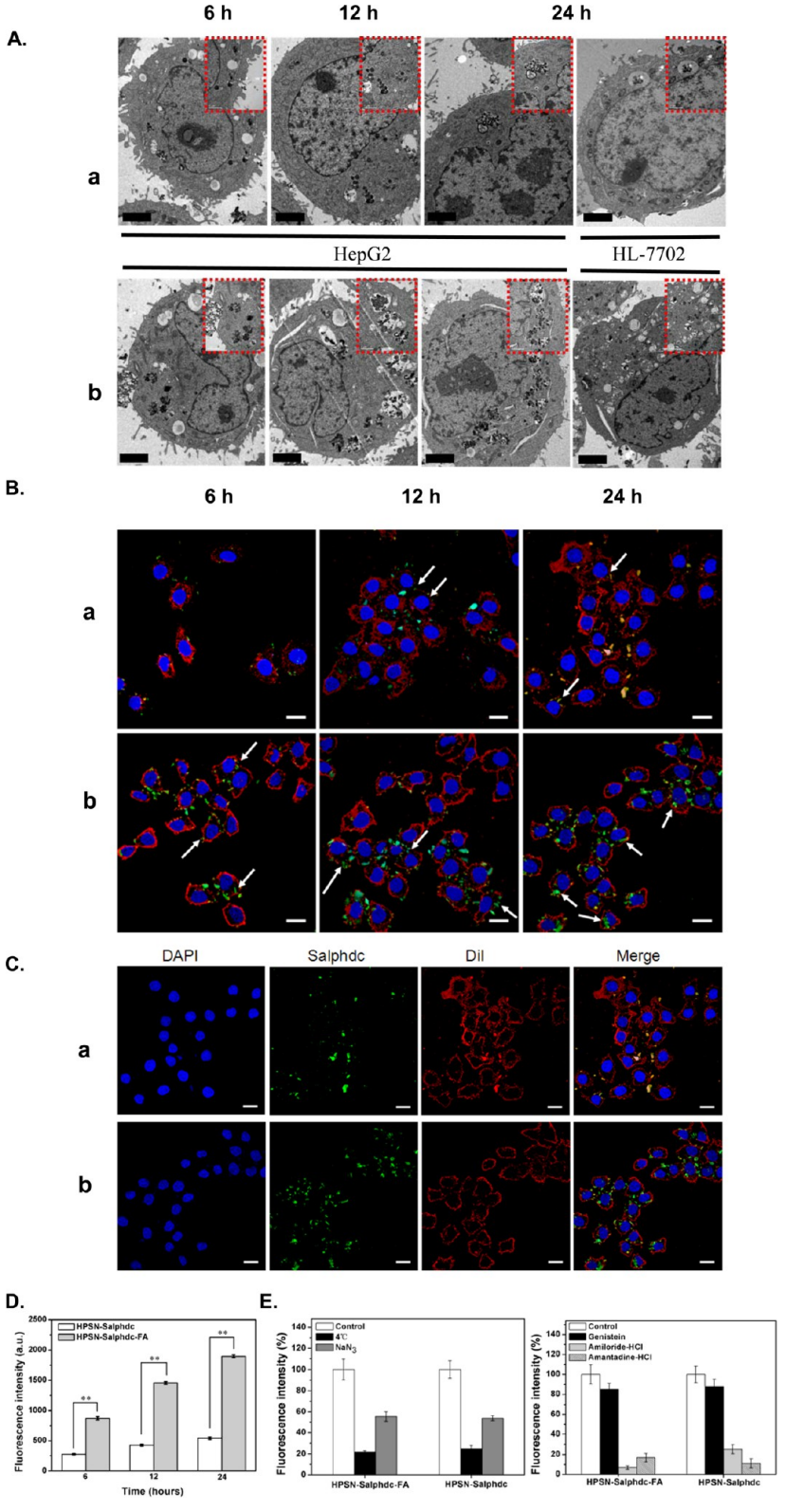

Figure 4. (A) TEM images of HepG2 cells treated with HPSN (a) and HPSN−Salphdc−FA (b) for 6, 12, and 24 h and that of HL-7702 cells with treatment for 24 h, respectively, showing the distributions of endocytosed nanoparticles within cells. The inserted images (dash frames) show the enlarged view of the endocytosed nanoparticles. Scar bar: 2 μm. (B) Cell morphology of HepG2 cells cocultured with HPSN−Salphdc (a) and HPSN−Salphdc−FA (b) for 6, 12, and 24 h, respectively. Cytomembrane (red, labeling with DiI) and cell nuclei (blue, labeling with DAPI). Scale bar: 20 μm. (C) CLSM images of endocytosed HPSN−Salphdc (a) and HPSN−Salphdc−FA (b) within HepG2 cells after treatment for 24 h. Images were taken from blue channel of DAPI, green channel of Salphdc, red channel of DiI, and merged channel (from left to right), respectively. Scale bar: 20 μm. (D) Fluorescence intensity analysis of Salphdc in HepG2 cells after treating with HPSN−Salphdc and HPSN−Salphdc−FA for 6, 12, and 24 h, respectively. (E) Quantification analysis the energy-dependent endocytosis (left) and other types endocytosis (right) of HPSN−Salphdc and HPSN−Salphdc−FA. The error bars indicate mean ± SD (n = 5), (**) $p < 0.01$.

DOI: 10.1021/acsami.5b00746
ACS Appl. Mater. Interfaces 2015, 7, 7357−7372

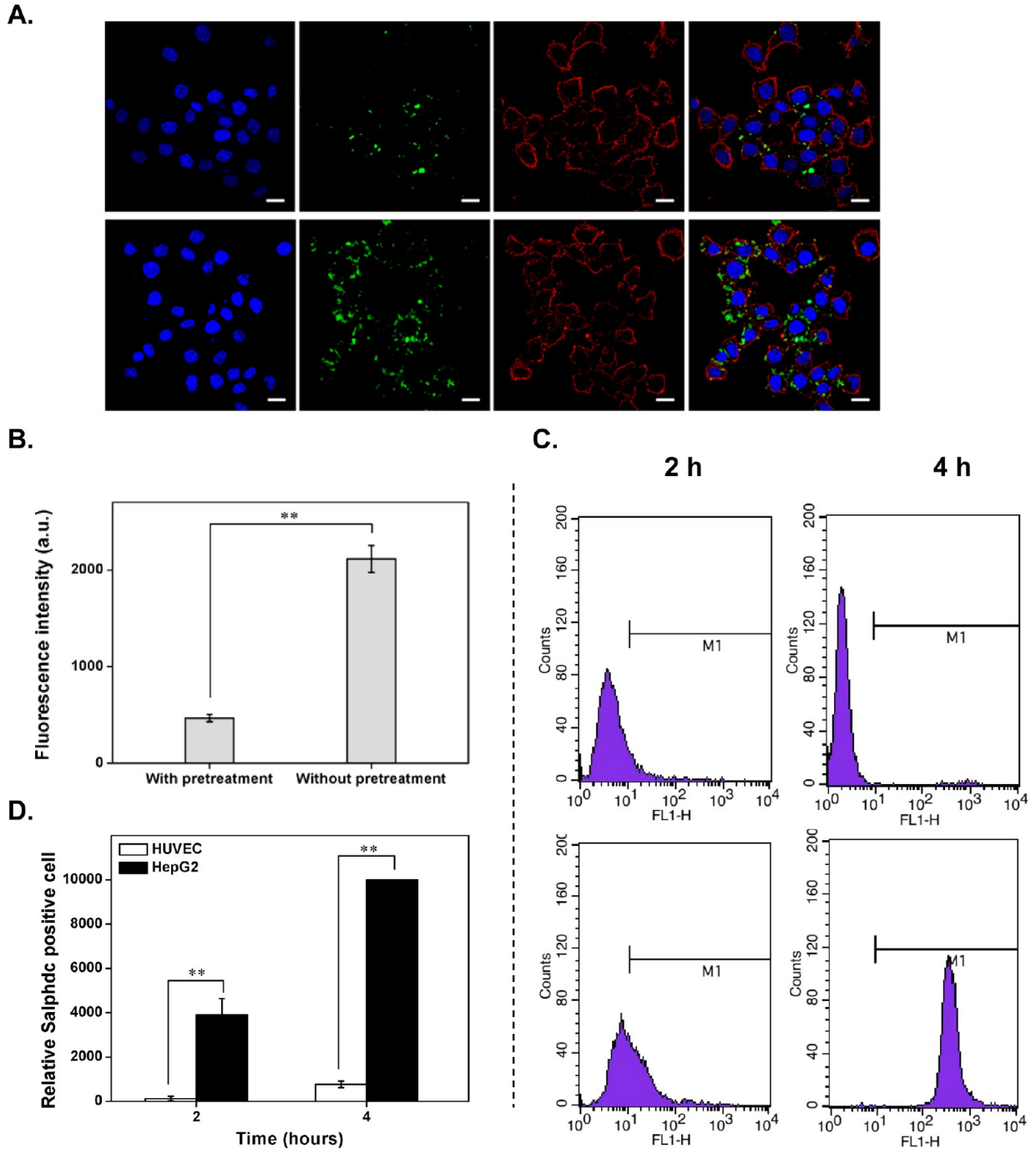

Figure 5. Cell specific endocytosis characterization: (A) CLSM images of HepG2 cells pretreated by FA (upper row) and free HPSN−Salphdc−FA (without FA pretreatment, lower row) for 24 h. (B) Fluorescence intensity analysis from part A. (C) Flow cytometry analysis of HepG2 cells (upper row) and HUVEC cells (lower row) for endocytosis level of HPSN−Salphdc−FA at different incubation times. (D) Quantification analysis based on part C. Scale bar: 20 μm. The error bars indicate mean ± SD (n = 3), (**) $p < 0.01$.

was significantly lower ($p < 0.01$) than that of HepG2 cells after culture for 2 and 4 h (Figure 5C and D). The result suggests that FA molecules conjugated with HPSN−Salphdc−FA was significantly important for cell endocytosis.

We also used CLSM to investigate the growth inhibition effect of DOX@HPSN−Salphdc−FA system on HepG2 cells after culture for 6, 12, and 24 h, respectively.[55,56] The integrity of nuclei structure was observed in HepG2 cells in spite of incubation time for TCPS group (control) (Figure 6A, a, a1, and a2). However, when treating with free DOX for 12 and 24 h, HepG2 cells displayed serious apoptosis (Figure 6A, b1 vs b2). Moreover, a slight apoptosis was shown on cells treated with DOX@HPSN for 12 and 24 h, respectively. It could be contributed to the delayed release of DOX from DOX@HPSN. Nevertheless, a more serious cell apoptosis was observed on cells treated with DOX@HPSN−Salphdc−FA than those of DOX and DOX@HPSN for 24 h rather than 12 h (Figure 6A, d2 vs b2, c2), mainly due to the inadequate effect of low pH, leading to the slight release of DOX in 12 h. The result suggests that the targeting effect of FA caused more DOX@HPSN−Salphdc−FA was endocytosed by HepG2, leading to more DOX release within HepG2 cells in a sustained behavior. It thus resulted in cell apoptosis.

DOI: 10.1021/acsami.5b00746
ACS Appl. Mater. Interfaces 2015, 7, 7357−7372

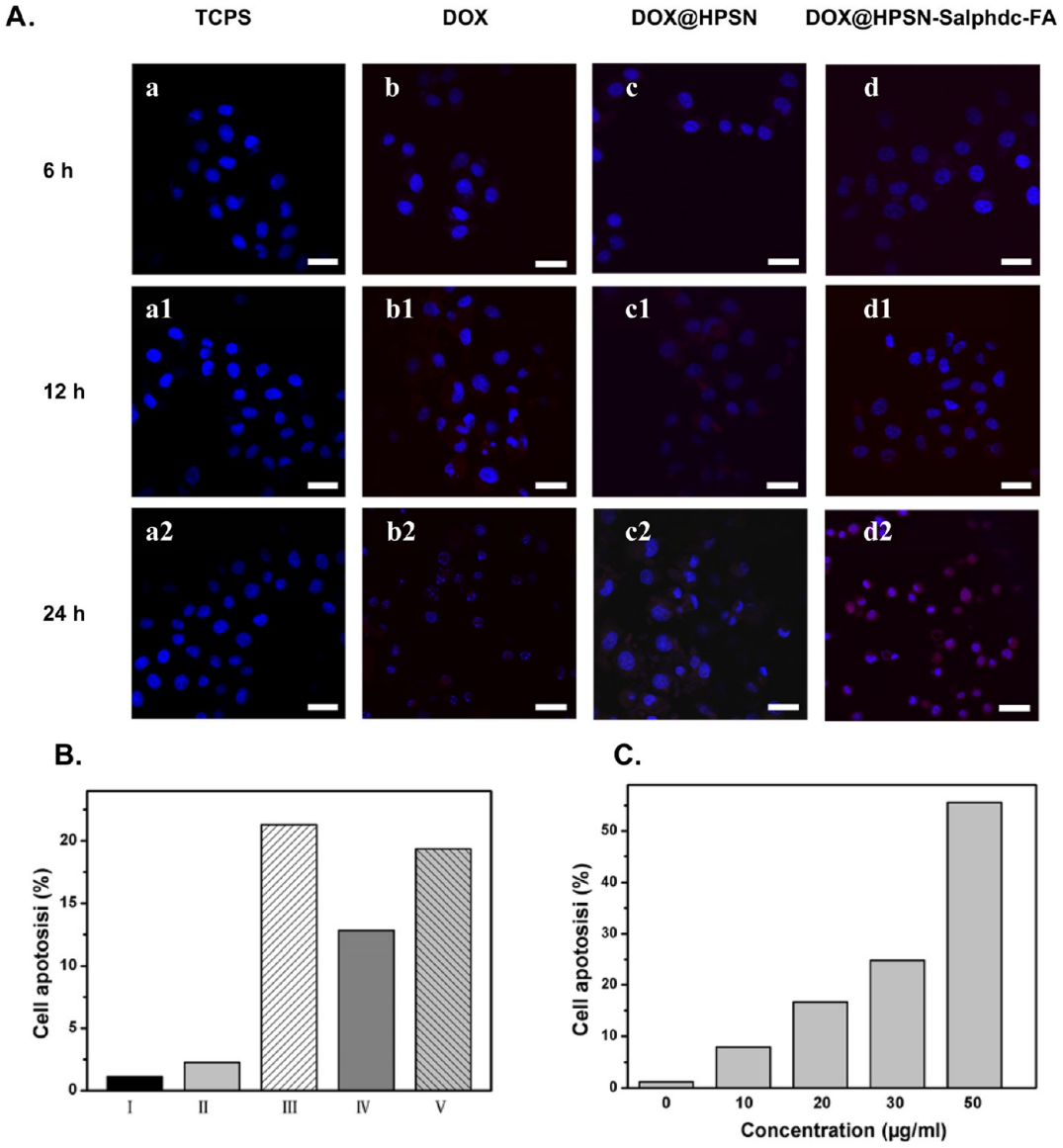

Figure 6. Cell apoptosis characterization in vitro. (A) Cell morphology of HepG2 cells cultured with (a) TCPS, (b) DOX, (c) DOX@HPSN, and (d) DOX@HPSN−Salphdc−FA for 6, 12, and 24 h, respectively. The red channel is from DOX, and the blue channel is from DAPI. Scale bars: 50 μm. (B) FCM assay of HepG2 cells treated with PBS (control, I) and 0.4 mg/mL of HPSN (II), 20 μg/mL of DOX (III) and equivalent amount of DOX loaded DOX@HPSN (IV), and DOX@HPSN−Salphdc−FA (V) for 24 h. (C) Quantitative apoptosis analysis of HepG2 cells treated with various concentrations of DOX@HPSN−Salphdc−FA for 24 h.

Subsequently, we used FCM to characterize the apoptosis level of HepG2 cells in vitro after treatment with HPSN−Salphdc−FA (Figure 6B, Figure S7A). It was observed that a negligible cell apoptosis because of the good biocompatibility of HPSN. In contrast, DOX or DOX loaded nanoparticles induced obvious cell apoptosis. Cells incubated with DOX@HPSN−Salphdc−FA displayed higher apoptosis than DOX@HPSN but lower than DOX. There were two reasons contributing to this phenomenon: on the one hand, a higher amount of DOX@HPSN−Salphdc−FA than DOX@HPSN were uptaken by HepG2 cells via FA targeting (Figure 5); on the other hand, soluble DOX directly acted against cells, while it would take time for DOX release from both DOX@HPSN−Salphdc−FA and DOX@HPSN.

Furthermore, we investigated the concentration-dependent apoptosis efficiency caused by DOX@HPSN−Salphdc−FA. After incubation for 24 h, the cell apoptosis increased when increasing the concentration of HPSN−Salphdc−FA (Figure 6C, Figure S7B). As for the high efficiency of DOX@HPSN−Salphdc−FA, the underlying mechanism was suggested as following: first, FA mediated cell specific endocytosis of DOX@HPSN−Salphdc−FA by HepG2 cells. Meanwhile, the end-capping of Salphdc could efficiently prevent the leakage of DOX from DOX@HPSN−Salphdc−FA before the system was uptaken into HepG2 cells; second, the linkage between Salphdc and HPSN were broken upon lower pH stimuli; third, a sustained delivery of DOX within HepG2 cells that induced cell apoptosis.

For in vivo study, we constructed a liver tumor bearing nude mouse model to investigate the curative effect of HPSN−Salphdc−FA system in vivo.[13] Figure 7A shows the optical images of tumors after subjection to 5 treatment groups. The tumors showed a rapid growth tendency after treatment with PBS and HPSN (control). However, DOX and DOX@HPSN treated tumor displayed slow growth tendency, comparing to

DOI: 10.1021/acsami.5b00746
ACS Appl. Mater. Interfaces 2015, 7, 7357−7372

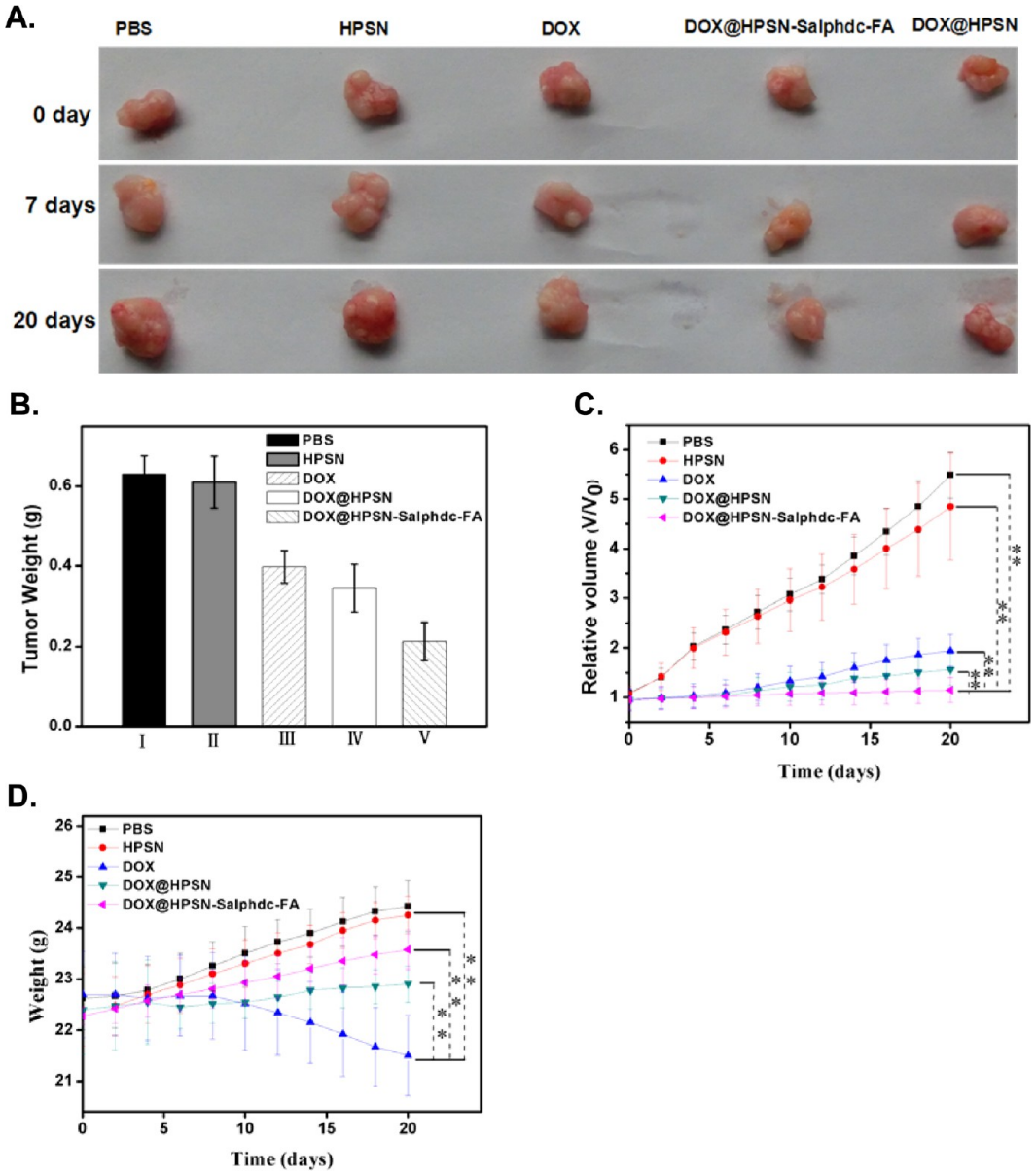

Figure 7. (A) Photo images of tumor tissues after treatment with PBS (control), HPSNs, DOX, DOX@HPSN, and DOX@HPSN−Salphdc−FA for 0, 7, and 20 days, respectively. Scale bars: 1 cm. (B) Final weights of tumor tissues of treating with drug/nanoparticles for 20 days. (C) Relative tumor volumes of nude mice after different treatments. (D) Weight analysis of mice of five groups. The error bars indicate mean ± SD (n = 4). (**) $p < 0.01$.

PBS (negative control) and HPSN (positive control). It implies that the tumor growth was inhibited by DOX and DOX@HPSN treatments, and curative effect of DOX@HPSN was better than that of free DOX. As for DOX@HPSN−Salphdc−FA group, it led to strong tumor suppression. The result of final tumor tissue weight also reflected the similar inhibition tendency (Figure 7B). These results clearly suggest that DOX@HPSN−Salphdc−FA had an excellent suppression effect on tumor growth.

Meanwhile, tumor volumes were measured to reflect the curative effects of different treatment on tumor growth. Tumor volumes of treatments with DOX and DOX@HPSN were increased slower than that of PBS (negative) and HPSN (positive) groups. Moreover, the DOX@HPSN−Salphdc−FA showed the greatest capability to inhibit the growth of tumor among all groups. After injection for 20 days, it could be observed that DOX@HPSN−Salphdc−FA group had the smallest ($p < 0.01$) tumor volume among all groups (Figure 7C), and a slightly inhibition effects were discovered with the treatment of free DOX. The reason could be implied that the half-life of DOX was short in body, in addition, DOX was rapidly diffused along with the blood circulation and only a little DOX reached to the tumor site.[57] In contrast, DOX@HPSN could delay the diffusion of DOX in body and improve the curative effect. Furthermore, DOX@HPSN−Salphdc−FA nanoparticles were accurately and quickly delivered and accumulated at tumor sites attribute to the targeting capability of FA. Then, sustained release of DOX was triggered by intracellular low pH value within tumor tissues and locally killed the tumor cells in vivo.

Besides, the mouse weights were also periodically recorded during the process of treatment. The mice of treatment with free DOX group showed a weight decrease tendency (21.5 g)

DOI: 10.1021/acsami.5b00746
ACS Appl. Mater. Interfaces 2015, 7, 7357−7372

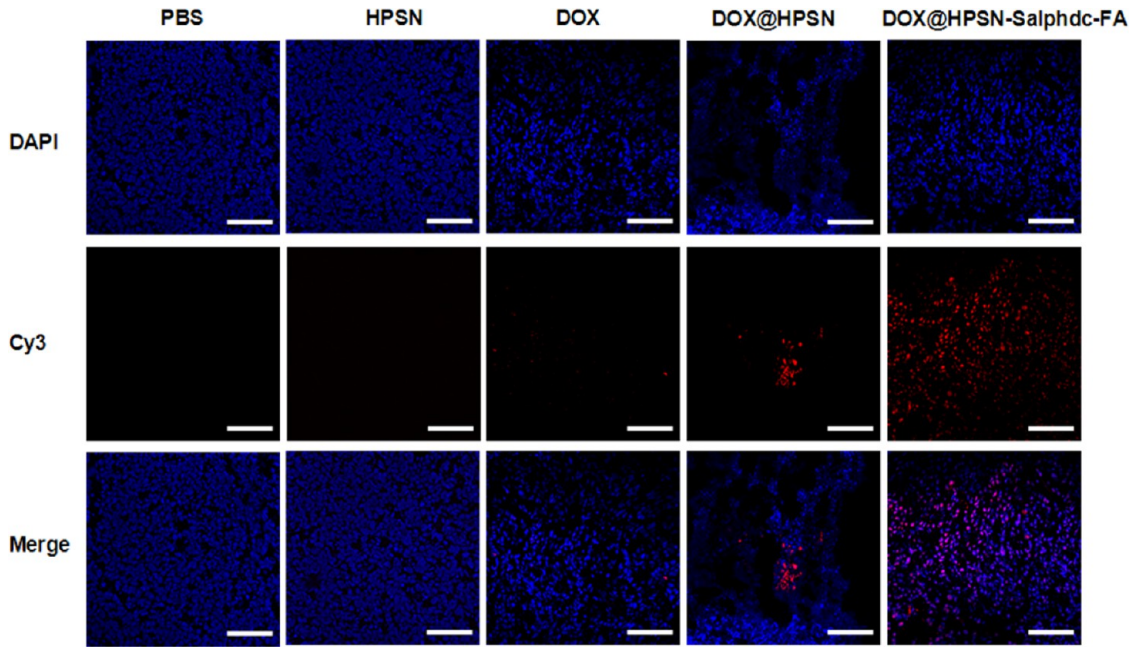

Figure 8. TUNEL staining observation: tumors were treated with PBS, HPSN, DOX, DOX@HPSN and DOX@HPSN−Salphdc−FA for 20 days. Images from up to down are blue channel from DAPI, red channel from Cy3, and merged channel, respectively. Cell nuclei were observed as blue dots and apoptotic DNA was visualized as magenta dots. Scale bars: 100 μm.

comparing with the initial weight. Nevertheless, the weights of mice treated PBS, HPSN, DOX@HPSN, and DOX@HPSN−Salphdc−FA increased and the final weights were around 24.4, 24.2, 23.8, 22.9, and 23.6 g, respectively (Figure 7D). These results demonstrate that HPSN−Salphdc−FA was a good drug delivery carrier which not only has good biocompatibility but also reduces the cytotoxicity of DOX to the normal tissue.[58]

Next, we used TUNEL enzymatic labeling and DAPI costaining assay was employed to reveal the inhibition mechanism of tumor tissues. The apoptosis cells (DNA) labeled with Cy3 and represented as the magenta dots (Figure 8). A slight and moderate apoptosis were observed for DOX and DOX@HPSN group, respectively. Comparing with the above groups, DOX@HPSN−Salphdc−FA group displayed high capability to induce tumor cells apoptosis, exhibiting by high level of the magenta dots. It suggests that DOX@HPSN−Salphdc−FA was a promising drug carrier for tumor therapy. It could be attributed to the targeting capability of FA and then the linkage between Salphdc and HPSN was broken by intracellular acidic pH, leading to a high concentration of DOX was release and accumulated in tumor sites to kill tumor cells.

To further investigate the clinical application potential of HPSN−Salphdc−FA, the status of major organs were investigated through the histological examination (Figure 9). The relevant tumor tissues were gathered after 20 day treatments with PBS, HPSNs, DOX, DOX@HPSN, and DOX@HPSN−Salphdc−FA, respectively. Then, the paraffin sections of those tissues were subjected to hematoxylin and eosin (HE) staining. Comparing with PBS (control) and HPSN groups, typical myocardial injury could be easily observed in the free DOX group, and an obvious reduction of heart injury was shown in the HPSN−Salphdc−FA@DOX group. Furthermore, it was friendly to the else normal tissues (spleen, kidney, liver, and lung) for HPSN−Salphdc−FA system. For tumor tissues, DOX@HPSN−Salphdc−FA induced the most serious damage comparing with other groups. With the result, it could be revealed that DOX@HPSN−Salphdc−FA system had good tumor curative effect with good biocompatibility for healthy organs.

To investigate whether the Salphdc-capped HPSN system could be used for bioimaging in vivo or not,[59] DOX@HPSN−Salphdc and DOX@HPSN−Salphdc−FA were injected into tumor-bearing mice. The fluorescence signals of the nanoparticles accumulating at tumor or other tissues were monitored with a Maestro system (CRi Inc.) (Figure 10A, Figure S8). The results suggest that most DOX@HPSN−Salphdc−FA nanoparticles accumulated at tumor tissue comparing with DOX@HPSN−Salphdc after postinjection for 3 h. With increasing time, the fluorescence levels of DOX@HPSN−Salphdc−FA nanoparticles in normal tissues gradually reduced, whereas it increased at tumor sites. Meanwhile, we also quantitatively measured the fluorescence signals of the tumors treated either with DOX@HPSN−Salphdc or DOX@HPSN−Salphdc−FA. The fluorescence intensity of tumor tissues treated with DOX@HPSN−Salphdc−FA was significantly higher ($p < 0.01$) than that of DOX@HPSN−Salphdc at each time of interval (Figure 10B). Moreover, the fluorescence intensity of tumor tissue was the highest for both for DOX@HPSN−Salphdc and DOX@HPSN−Salphdc−FA treated mice after postinjection for 16 h. The fluorescence intensity then gradually weakened along with time increasing. The reason could be implied as follows: first, the intravenously injected DOX@HPSN−Salphdc and DOX@HPSN−Salphdc−FA nanoparticles distributed in the whole body via blood circulation;[60,61] second, those nanoparticles could be accumulated at tumor sites through EPR effect.[62] As for DOX@HPSN−Salphdc−FA, the targeting moiety of FA further resulted in the accumulation of DOX@HPSN−Salphdc−FA at tumor site via a receptor recognition pathway, in turn led to the higher fluorescence intensity than that of DOX@HPSN−Salphdc; third, the coordination bonds connecting fluorescent Salphdc with HPSN were cleaved under intracellular acidic condition, thus leading to the fluorescence weakened gradually.

DOI: 10.1021/acsami.5b00746
ACS Appl. Mater. Interfaces 2015, 7, 7357−7372

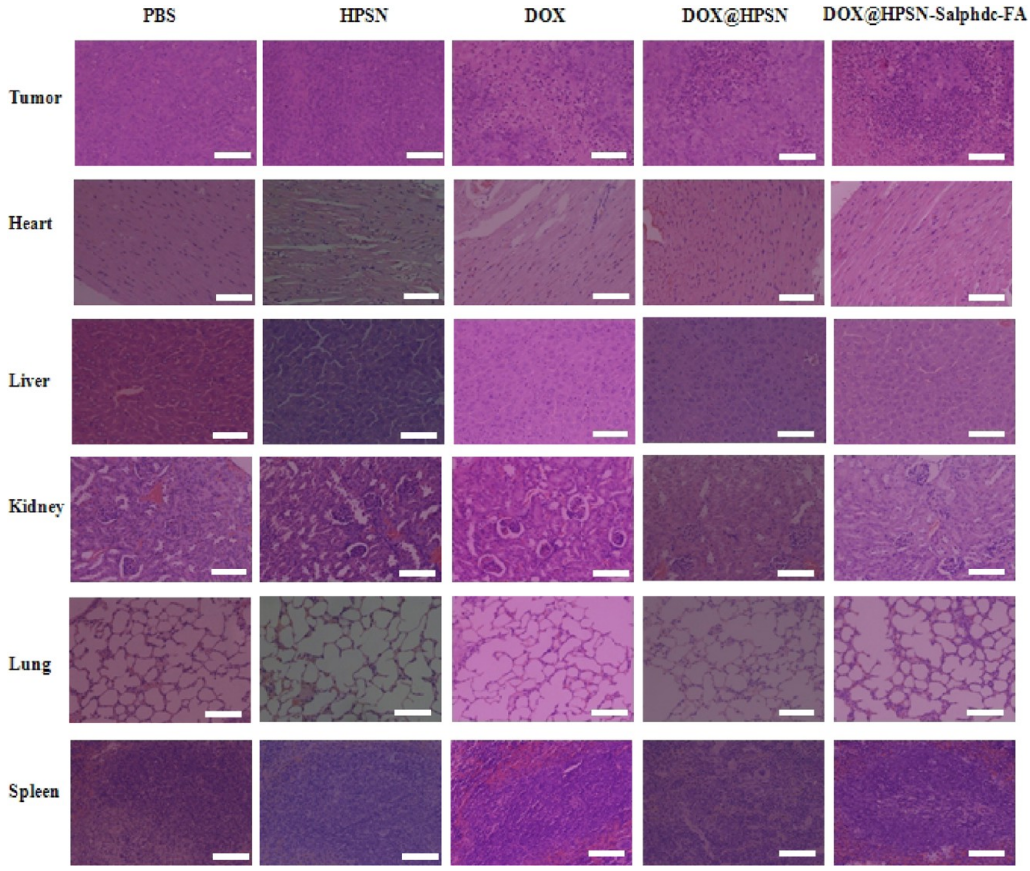

Figure 9. Histopathological observation of different organs (spleen, tumor, kidney, liver, lung, and heart) from tumor-bearing mice. Scale bars: 100 μm.

After injection for 48 h, the fluorescence signals of both nanoparticles were still visualized. The reason is that the complete clearance of nanoparticles from body generally takes time. Previously, Park et al. confirmed that the clearance of Si nanoparticles accumulating at organs of mice took 4 weeks.[63]

Moreover, after postinjection of DOX@HPSN−Salphdc−FA for 16 h, the treated mice were sacrificed for fluorescence imaging to evaluate the nanoparticles distribution in tissues (spleen, tumor, kidney, liver, lung, and heart; Figure 10C). The quantitative Si energy-dispersive spectrometry (EDS) analysis displayed that of the accumulation of DOX@HPSN−Salphdc−FA at tumor tissue was much higher than those of normal tissues: heart (21.2-fold), liver (2.61-fold), spleen (4.59-fold), lung (2.8-fold), and kidney (4.1-fold) (Figure 10D, and Figure S9). The EDS analysis of In element displayed similar trend to that of Si element.

Finally, normal nude mice were chosen to investigate the blood circulation of DOX@HPSN−Salphdc and DOX@HPSN−Salphdc−FA nanoparticles which were intravenously injected. The fluorescence intensities of both nanoparticles in blood were detected at each time of interval (Figure 10E). It shows that no significant differences between them and the blood clearance curves of both nanoparticles were accordance with the two-compartment model. Furthermore, the half-lives of DOX@HPSN−Salphdc were 7.96 and 588.62 min, and 7.87 and 606.34 min for DOX@HPSN−Salphdc−FA. All results demonstrate that the HPSN−Salphdc−FA carrier was a promising drug delivery system with bioimaging. In short, we confirmed the hypothesis that DOX@HPSN−Salphdc−FA system was an efficient carrier for pH-responsive targeted drug delivery with bioimaging potential.

CONCLUSION

In short, we designed and developed a smart and biocompatible HPSN-based drug delivery system with great curative effect on tumor growth and bioimaging potential. Various techniques such as TEM, BET, TGA, etc., proved the successful fabrication of the system. The DOX@HPSN−Salphdc−FA system demonstrated pH-responsive targeted drug delivery in vitro and in vivo tumor therapy. The potential pathway of cell endocytosis was revealed. Meanwhile, the system only displayed minimal toxic side effect on normal organs. Furthermore, the DOX@HPSN−Salphdc−FA system demonstrated great potential for biological imaging in vivo. The study affords an alternative for the development of drug delivery carrier for imaging-guided tumor therapy.

EXPERIMENTAL SECTION

Materials. Tluoresceinisothiocynate (FITC), doxorubicin hydrochloride (DOX·HCl), 1-ethyl-3-(3-(dimethylamino)propyl) carbodiimidehydrochloride (EDC·HCl), tetraethyl orthosilicate (TEOS), 3-aminopropyltriethoxysilane (APTES), and *N*-hydroxysuccinimide (NHS) were provided by Sigma-Aldrich (Beijing, China). Folic acid dihydrate (FA), succinic anhydride (SA), and *N*-cetyltrimethylammonium bromide (CTAB) were purchased from Alfa Aesar (Tianjin, China). 3-Formyl-4-hydroxybenzoic acid was supplied by Hanhong Chemical Chemical Co Ltd. (Chongqing, China). *o*-Phenylenediamine and *N*,*N*-dimethylformamide were supplied by J&K Scientific Ltd. Tetrahydrofuran (THF), and indium nitrate hydrate ($In(NO_3)_3 \cdot xH_2O$) was provided by Aladdin Industrial Co Ltd. Ethyl ether and triethanolamine (TEA) were bought from Chuandong Chemical Co Ltd. Other chemicals were provided by Oriental Chemicals Co Ltd. All the reagents were analytical grade.

DOI: 10.1021/acsami.5b00746
ACS Appl. Mater. Interfaces 2015, 7, 7357−7372

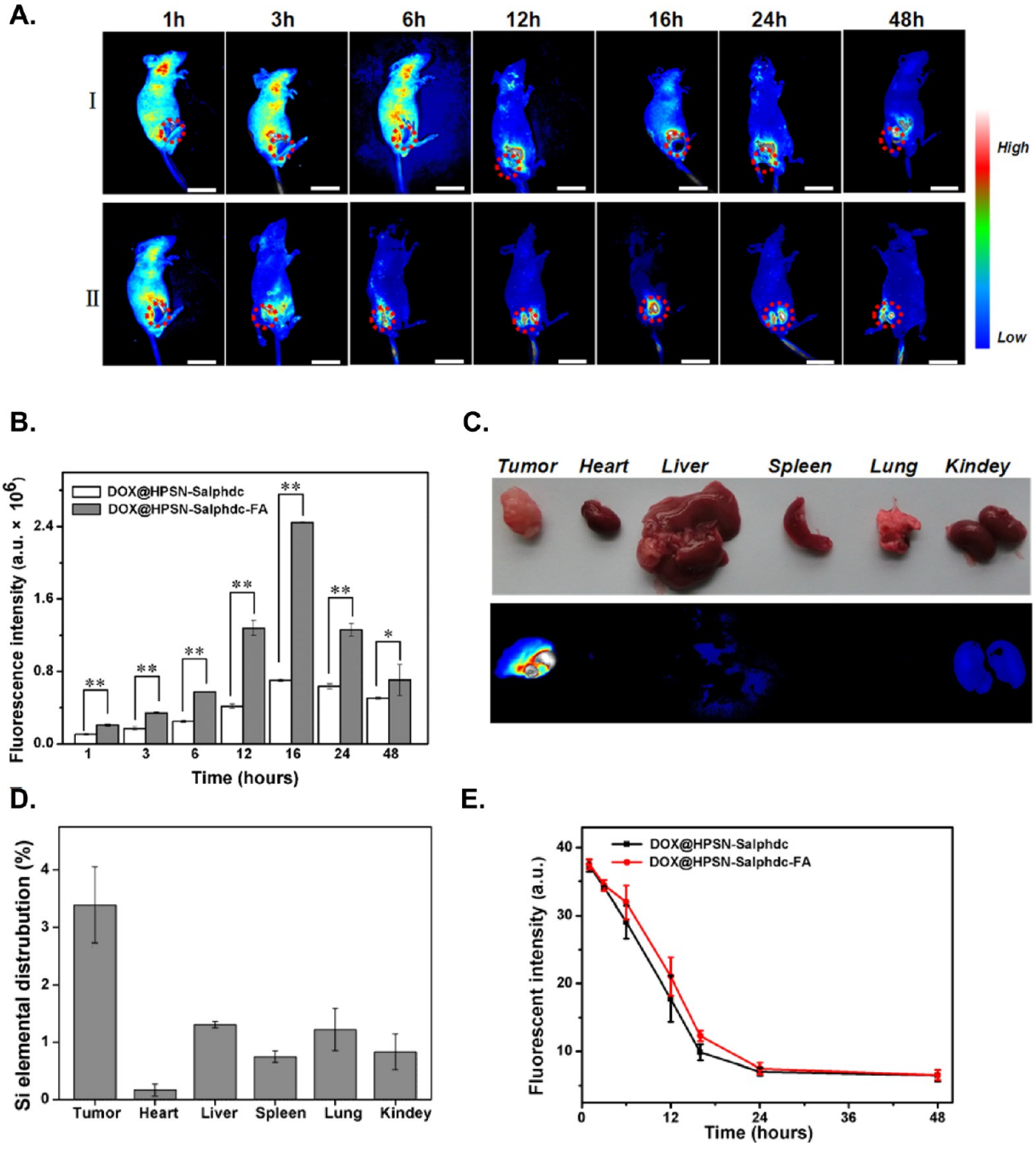

Figure 10. (A) Whole-body real-time fluorescence imaging of DOX@HPSN−Salphdc (I) and DOX@HPSN−Salphdc−FA (II) for 1, 3, 6, 12, 16, 24, and 48 h, respectively. The dash cycles represent the tumor locations. Scale bars: 3 cm. (B) Histogram of the fluorescence intensity of tumors after injection of DOX@HPSN−Salphdc and DOX@HPSN−Salphdc−FA for 1, 3, 6, 12, 16, 24, and 48 h, respectively. (C) Images of mainly organs (spleen, tumor, kidney, liver, lung, and heart) after injection of DOX@HPSN−Salphdc−FA for 16 h. (D) Quantitative energy dispersive spectrometry analysis of Si element of tumor and normal organs subjected to DOX@HPSN−Salphdc−FA for 16 h. (E) Blood clearance curves of DOX@HPSN−Salphdc and DOX@HPSN−Salphdc−FA in normal nude mice. The error bars indicate mean ± SD (n = 4). (*) $p < 0.05$ and (**) $p < 0.01$.

Synthesis and Functionalization of Dendrimerlike Silica Nanoparticles. The HPSN was synthesized based on a previous study.[44] Typically, a mixture solution containing distilled water (70 mL), CTAB (0.5 g), aqueous ammonia (0.8 mL), ethanol (5 mL), and ethyl ether (15 mL) was stirred at 15 °C for 30 min. After that, mixture solution containing APTES (0.1 mL) and TEOS (2.5 mL) was added and stirred at 15 °C for another 4 h. Next, 1 mL of HCl (37%) was added to the solution so as to stop the base-catalyzed reaction. The nanoparticles were collected through centrifugation.

The as-synthesized nanoparticles were purified by gradient centrifugation. First, the product was dispersed into ethanol (100 mL) and treated by ultrasonic dispersion. The nanoparticle suspension was treated by centrifuging with various speeds (3000, 3200, and 4200 rpm) to remove large particles. Finally, the purified nanoparticles were obtained by centrifuging with 4200 rpm for 12 min. The purified nanoparticles were dried at 60 °C for analysis.

The above obtained nanoparticles were dissolved into a mixture solution containing HCl (7 mL) and methanol (120 mL). The reaction was allowed to last at 80 °C for 24 h. Then, to remove the large particles, the solution was centrifuged at 4200 rpm for 12 min and collected the extracted nanoparticles. The purified and extracted nanoparticles (HPSN−NH_2) were kept in distilled water or DMF for further use.

DOI: 10.1021/acsami.5b00746
ACS Appl. Mater. Interfaces 2015, 7, 7357−7372

Carboxyl-functionalized HPSNs were synthesized based on a previous report.[46] A 50 mg portion of HPSN−NH_2 was added to 20 mL of DMF and dispersed by ultrasonic treatment. The solution containing SA (0.45 g) and DMF (5 mL) was added. Afterward, TEA (0.45 mL) was poured and catalyzed the reaction. The solution was stirred at ambient temperature for 12 h. HPSN−COOH was obtained by centrifugation and then dispersed into water for further use.

Synthesis of *N,N*-Phenylenebis(salicylideneimine)dicarboxylic Acid (Salphdc). Salphdc was synthesized based on a previous report.[64] Typically, Fhba (1.08 g) was dissolved into ethanol (100 mL) solution. Then, *o*-phenylenediamine solution (0.352 g) in ethanol (100 mL) was added to the solution above. The reaction was lasted at 60 °C for 24 h. After that, the Salphdc product was obtained, rinsed with ethanol and THF 6 times each, and dried with lyophilization.

Drug Loading. Typically, HPSN−COOH (60 mg) was dispersed with PBS buffer (60 mL, 0.1 M, pH 5.0) solution. Then, DOX (6 mg) was added and stirred at ambient temperature for 24 h. The obtained substance was collected by centrifugation, which was denoted as DOX@HPSN and used for subsequent experiments.

Synthesis of Salphdc-Capped Dendrimerlike Silica Nanoparticles. Salphdc was used to seal HPSN-COOH and/or DOX@HPSN.[47] Briefly, The Salphdc (60 mg, 150 mmol) and $In(NO_3)_3 \cdot xH_2O$ (44.7 mg, 150 mmol) were dissolved into 40 mL DMF to form a yellow solution, to which 80 mg of HPSN-COOH was added. The above precursor mixture was ultrasonically treated and transferred to a 100 mL three-necked flask, and then stirred vigorously at 120 °C. The reaction was lasted for 15 min until the precipitate was gradually formed in the mixture solution. After cooling to ambient temperature, the nanoparticles were obtained through centrifugation and dried with lyophilization. The nanoparticles were named as HPSN−Salphdc. If DOX was loaded, the nanoparticles were named as DOX@HPSN−Salphdc.

Conjugation of FA to HPSN−Salphdc. HPSN−Salphdc was activated based on a previous study.[65] HPSN−Salphdc (60 mg), EDC (30 mg) and NHS (15 mg) were added to 10 mL DMSO solution upon stirring at room temperature for 2 h. DMSO (8 mL) containing FA (80 mg) was poured into above solution upon stirring at ambient temperature for 24 h. The resulting particles were collected via centrifugation and dried with lyophilization. The obtained nanoparticles were named as HPSN−Salphdc−FA. The resulting substance was denoted as DOX@HPSN−Salphdc−FA if DOX was loaded.

Material Characterization. Morphologies of HPSN and HPSN−Salphdc−FA were observed with TEM (LIBRA 200 CS, Carl Zeiss Co., Germany) and field emission scanning electron microscopy (FEI Nova 400 Nano SEM, Phillips Co., Holland), respectively. Energy dispersive X-ray spectroscopy (EDS) was used for chemistry analysis. BET was employed to characterize surface areas of various materials, and BJH (ASAP2020M, USA) was used to observe the size distributions of different materials. FTIR (model 6300, Bio-Rad Co. Ltd., USA), HNMR spectrometer (AV500 MHz, Bruker, Swiss), zeta potential measurements (Nano ZS90 Zetasizer, Malvern Instruments Co. Ltd., UK) equipped with DLS, and thermal gravimetric analysis (TGA, DTG 60H, Japan) were employed to characterize the functionalization, respectively.

Drug Release. Briefly, DOX@HPSN−Salphdc−FA (0.75 mg) nanoparticles were dispersed into 8 mL PBS solutions with various pH values (7.4 and 5.0) and poured into a dialysis bag (MWC 8000). Then, the tubes were immersed into 40 mL of PBS with different pH values and stirred at 37 °C. Then, 0.8 mL solution supernatant was taken out and analyzed with UV/vis/NIR (Lambda 900, PerkinElmer instruments, USA, excitation = 480 nm) spectrometer at different times. Meanwhile, the same volume of PBS was added to the solution. The loading degree and encapsulation efficiency was determined by following equations:

$$\text{loading degree (\%)} = \frac{\text{amount of loaded DOX}}{\text{total weight (HPSN−Salphdc−FA + DOX)}} \times 100\%$$

$$\text{encapsulation efficiency (\%)} = \left[1 - \frac{\text{drug in supernatant liquid}}{\text{total drug added}}\right] \times 100\%$$

Cell Culture. Normal human liver cells (HL-7702), HUVEC, and HepG2 cells were incubated with RPMI1640 medium composing fetal bovine serum (FBS, 10 vol %), penicillin (100 U/mL), and streptomycin (100 μg/mL) with a humid atmosphere containing 5% CO_2 at 37 °C.

Cell Viability. Cells were incubated with HPSN and HPSN−Salphdc−FA nanoparticles in 24-well plates for 6, 12, 24, and 48 h, respectively. The concentration of nanoparticles was adjusted to 0.4 mg/mL. The cell seeding density was 2×10^4 cells/cm^2. Then, the mixture solution containing 200 μL new medium and 20 μL CCK-8 was poured into each well with incubating for 1.5 h. The solution was measured with a spectrophotometric microplate reader (Bio-Rad 680, USA) at 450 nm.

Morphology Visualization. HepG2 cells were incubated with HPSN−Salphdc and HPSN−Salphdc−FA for 6, 12, and 24 h, respectively. The cell density was 10^5/cm^2. Subsequently, the cells were fixed with 4% para-formaldehyde at 4 °C for 24 h. Then, the samples were washed with PBS and stained with DiI (10 mM) and DAPI (20 μg/mL). Finally, the stained cells were observed with CLSM (LSM 510 META Olympus, Japan).

Endocytosis Mechanism Assay. One group of HepG2 cells were cultured with HPSN−Salphdc or HPSN−Salphdc−FA particles at 37 or 4 °C for 2 h, respectively. Meanwhile, we used sodium azide to treat another group of HepG2 cells for 1 h. And then all above group cells were collected to analyze the fluorescence intensity of treatment groups. Next, HepG2 cells were treated with others endocytosis inhibitors (100 mM of genistein, 2.5 mM of amiloride−HCl, and 1 mM of amantadine−HCl) for 1 h before incubation with HPSN−Salphdc or HPSN−Salphdc−FA particles for 2 h. Then, all cells were collected and analyzed fluorescence intensity.

Flow Cytometry Assay. HepG2 cells were cocultured with TCPS (control), HPSNs, DOX, DOX@HPSN, and DOX@HPSN−Salphdc−FA for 24 h. Cells were then harvested and resuspended in cell binding solution (Annexin V-FITC kit of NeoBioscience). Next, the cell of binding solution were subsequently treated with Annexin V-FITC (5 μL) and PI (10 μL) for 10 min in dark. Finally, the solution was removed to tubes and analyzed with FACS Calibur (BD Biosciences).

The endocytosis level of HepG2 and HUVEC cells for HPSN−Salphdc−FA carrier were also analyzed with FCM. Both cells were treated with HPSN−Salphdc−FA for 2 and 4 h, respectively. The concentration of nanoparticles was 0.4 mg/mL. After treatment, cells were collected and resuspended in binding buffer. Next, the solution was removed to tubes and analyzed with FACS Calibur.

Tumor Model. All male nude mice (4−6 weeks old) were supplied by of Xinqiao Hospital's Animal laboratory. The tumor model was established by subcutaneously injection of PBS (100 μL, pH 7.2) solution suspended with 2×10^6 HepG2 cells at the groin side of each nude mouse. All animal surgeries were conformed to the protocol of Institutional Animal Care and Use Committee of China. The mice were seeded for 7−10 days until the tumor volume reached around 50 mm^3.

In vivo Tumor Therapy. The mice were divided to five groups (n = 4/group) based on their similar tumor volumes and body weights. Then, the mice were injected with drug or nanoparticles (PBS, HPSN, DOX, DOX@HPSN, and DOX@HPSN−Salphdc−FA) via the tail vein of mice. The dose of DOX was 3 mg/kg day. The weight of body and size of tumor were recorded per 2 days, the following equation was employed to calculate tumor volume:

$$\text{tumor volume } (V) = \text{length} \times \text{width} \times \text{width}/2$$

Histological Assay. All mice were sacrificed after treatments for 20 days. Then, the main organs including heart, kidney, lung, spleen, and liver, as well as tumor tissue were collected and fixed with 10% formalin at 4 °C for 48 h. Next, the fixed organs/tumor tissue were

DOI: 10.1021/acsami.5b00746
ACS Appl. Mater. Interfaces 2015, 7, 7357−7372

embedded with paraffin and sectioned for hematoxylin and eosin (HE) staining. The stained slices were visualized with an optical microscope.

TUNEL Staining. Typically, tumor sections were pretreated with deparaffin and protease K, and then stained with TUNEL solutions (50 μL/section) and DAPI (20 μg/mL), respectively. Finally, CLSM (LSM 510 META Olympus, Japan) was employed to visualize the sections.

In vivo Fluorescence Imaging. Nude mice were injected different HPSN nanoparticles via tail vein. The mice were anesthetized with pelltobarbitalum natricum at the appointed time for fluorescence imaging, which was visualized with a Maestro system (CRi Inc.). The background fluorescence was removed via a filter parameter (excitation = 469/35 nm; emission = 518/42 nm), and then imaged with a filter parameter (excitation = 440/40 nm; emission = 518/42 nm) .

Blood Clearance Assay. Normal nude mice were chosen to investigate the blood circulation of DOX@HPSN−Salphdc and DOX@HPSN−Salphdc−FA nanoparticles which were intravenously injected. After 1, 3, 6, 12, 16, 24, and 48 h postinjection, the blood was obtained from the orbital sinus of the mouse and then measured using a Maestro fluorescence imaging system (Maestro1.0, USA).

Statistical Analysis. A form of means ± standard deviation (SD) was used to express all statistical data. OriginPro (version 8.0) was utilized for statistical analysis. Student's *t* test and one-way analysis of variance (ANOVA) was analyzed in this study. The confidence levels of 95% and 99% were regarded as significant difference.

■ ASSOCIATED CONTENT

Ⓢ Supporting Information

Particle size distributions (DLS), SEM and TEM images of different HPSNs, BET and BJH parameters and curves of different HPSNs, FITR and HNMR spectra of different HPSNs, TEM images of cell endocytosis, flow cytometry analysis, whole-body fluorescence imaging, element analysis, and Zeta-potentials of different HPSNs. This material is available free of charge via the Internet at http://pubs.acs.org/.

■ AUTHOR INFORMATION

Corresponding Author

*E-mail: kaiyong_cai@cqu.edu.cn.

Author Contributions

All authors contributed to the writing of the manuscript. All authors have approved the final version of manuscript.

Notes

The authors declare no competing financial interest.

■ ACKNOWLEDGMENTS

We thank the National Natural Science Foundation of China (31170923 and 21274169), Natural Science Foundation of Chongqing Municipal Government (CSTC2013kjrc-ljrcpy0004 and CSTC2013jjB50004), and the "111" project (B06023) for financial support.

■ REFERENCES

(1) Pan, H. M.; Grow, M. E.; Wilson, O.; Daniel, M. C. A New Poly (propylene imine) Dendron as Potential Convenient Building-block in the Construction of Multifunctional Systems. *Tetrahedron* **2013**, *69*, 2799−2806.

(2) Daniel, M. C.; Grow, M. E.; Pan, H. M.; Bednarek, M.; Ghann, W. E.; Zabetakisa, K.; Cornish, J. Gold Nanoparticle-cored Poly-(propyleneimine) Dendrimers as a New Platform for Multifunctional Drug Delivery Systems. *New J. Chem.* **2011**, *35*, 2366−2374.

(3) Connal, L. A.; Vestberg, R.; Hawker, C. J.; Qiao, G. G. Synthesis of Dendron Functionalized Core Cross-linked Star Polymers. *Macromolecules* **2007**, *40*, 7855−7863.

(4) Liong, M.; Lu, J.; Kovochich, M.; Xia, T.; Ruehm, S. G.; Nel, A. E.; Tamanoi, F.; Zink, J. I. Multifunctional Inorganic Nanoparticles for Imaging, Targeting, and Drug Delivery. *ACS Nano* **2008**, *2*, 889−896.

(5) Lee, J. E.; Lee, N.; Kim, H.; Kim, J.; Choi, S. H.; Kim, J. H.; Kim, T.; Song, I.; Park, S. P.; Moon, W.; Hyeon, T. Uniform Mesoporous Dye-doped Silica Nanoparticles Decorated with Multiple Magnetite Nanocrystals for Simultaneous Enhanced Magnetic Resonance Imaging, Fluorescence Imaging, and Drug Delivery. *J. Am. Chem. Soc.* **2010**, *132*, 552−557.

(6) Luo, Z.; Cai, K. Y.; Hu, Y.; Zhang, B. L.; Xu, D. W. Cell-specific Intracellular Anticancer Drug Delivery from Mesoporous Silica Nanoparticles with pH Sensitivity. *Adv. Healthcare Mater.* **2012**, *1*, 321−325.

(7) Muhammad, F.; Wang, A. F.; Guo, M. Y.; Zhao, J. Y.; Qi, W. X.; Guo, Y. J.; Gu, J. K.; Zhu, G. S. pH Dictates the Release of Hydrophobic Drug Cocktail from Mesoporous Nanoarchitecture. *ACS Appl. Mater. Interfaces* **2013**, *5*, 11828−11835.

(8) Zhang, G. L.; Yang, M. L.; Cai, D. Q.; Zheng, K.; Zhang, X.; Wu, L. F.; Wu, Z. Y. Composite of Functional Mesoporous Silica and DNA: An Enzyme-Responsive Controlled Release Drug Carrier System. *ACS Appl. Mater. Interfaces* **2014**, *6*, 8042−8047.

(9) Zhu, L.; Wang, T.; Perche, F.; Taigind, A.; Torchilin, V. P. Enhanced Anticancer Activity of Nanopreparation Containing an MMP2-Sensitive PEG-drug Conjugate and Cell-penetrating Moiety. *Proc. Natl. Acad. Sci. U.S.A.* **2013**, *110*, 17047−17052.

(10) Liu, T. Y.; Liu, K. H.; Liu, D. M.; Chen, S. Y.; Chen, I. W. Temperature-Sensitive Nanocapsules for Controlled Drug Release Caused by Magnetically Triggered Structural Disruption. *Adv. Funct. Mater.* **2009**, *19*, 616−623.

(11) Fedoryshin, L. L.; Tavares, A. J.; Petryayeva, E.; Doughan, S.; Krull, U. J. Near-Infrared-Triggered Anticancer Drug Release from Upconverting Nanoparticles. *ACS Appl. Mater. Interfaces* **2014**, *6*, 13600−13606.

(12) Dai, L. L.; Li, J. H.; Zhang, B. L.; Liu, J. J.; Luo, Z.; Cai, K. Y. Redox-Responsive Nanocarrier Based on Heparin End-capped Mesoporous Silica Nanoparticles for Targeted Tumor Therapy *in Vitro* and *in Vivo*. *Langmuir* **2014**, *30*, 7867−7877.

(13) Luo, Z.; Ding, X. W.; Hu, Y.; Wu, S. J.; Xiang, Y.; Zeng, Y. F.; Zhang, B. L.; Yan, H.; Zhang, H. C.; Zhu, L. L.; Liu, J. J.; Li, J. H.; Cai, K. Y.; Zhao, Y. L. Engineering a Hollow Nanocontainer Platform with Multifunctional Molecular Machines for Tumor-targeted Therapy *in Vitro* and *in Vivo*. *ACS Nano* **2013**, *7*, 10271−10284.

(14) Zhang, B. L.; Luo, Z.; Liu, J. J.; Ding, X. W.; Li, J. H.; Cai, K. Y. Cytochrome C End-capped Mesoporous Silica Nanoparticles as Redox-responsive Drug Delivery Vehicles for Liver Tumor-targeted Triplex Therapy *in Vitro* and *in Vivo*. *J. Controlled Release* **2014**, *192*, 192−201.

(15) Du, X.; Shi, B. Y.; Liang, J.; Bi, J. X.; Dai, S.; Qiao, S. Z. Developing Functionalized Dendrimer-like Silica Nanoparticles with Hierarchical Pores as Advanced Delivery Nanocarriers. *Adv. Mater.* **2013**, *25*, 5981−5985.

(16) Jana, A.; Nguyen, K. T.; Li, X.; Zhu, P. C.; Tan, N. S.; Ågren, H.; Zhao, Y. L. Perylene-derived Single-component Organic Nanoparticles with Tunable Emission: Efficient Anticancer Drug Carriers with Real-time Monitoring of Drug Release. *ACS Nano* **2014**, *8*, 5939−5952.

(17) Hu, Y.; Cai, K. Y.; Luo, Z.; Jandt, K. D. Layer-By-Layer Assembly of Beta-estradiol Loaded Mesoporous Silica Nanoparticles on Titanium Substrates and Its Implication for Bone Homeostasis. *Adv. Mater.* **2010**, *22*, 4146−4150.

(18) Meng, H.; Xue, M.; Xia, T.; Zhao, Y. L.; Tamanoi, F.; Stoddart, J. F.; Zink, J. I.; Nel, A. E. Autonomous in Vitro Anticancer Drug Release from Mesoporous Silica Nanoparticles by pH-Sensitive Nanovalves. *J. Am. Chem. Soc.* **2010**, *132*, 12690−12697.

(19) Rim, H. P.; Min, K. H.; Lee, H. J.; Jeong, S. Y.; Lee, S. C. pH-tunable Calcium Phosphate Covered Mesoporous Silica Nanocontainers for Intracellular Controlled Release of Guest Drugs Mesoporous Silica Nanoparticles End-capped with Collagen: Redox-responsive Nanoreservoirs for Targeted Drug Delivery. *Angew. Chem., Int. Ed.* **2011**, *50*, 8853−8857.

DOI: 10.1021/acsami.5b00746
ACS Appl. Mater. Interfaces 2015, 7, 7357−7372

(20) Chen, Z. W.; Li, Z. H.; Lin, Y. H.; Yin, M. L.; Ren, J. S.; Qu, X. G. Biomineralization Inspired Surface Engineering of Nanocarriers for pH-responsive, Targeted Drug Delivery. *Biomaterials* **2013**, *34*, 1364−1371.
(21) Zhang, Q.; Liu, F.; Nguyen, K. T.; Ma, X.; Wang, X. J.; Xing, B. G.; Zhao, Y. L. Multifunctional Mesoporous Silica Nanoparticles for Cancer-targeted and Controlled Drug Delivery. *Adv. Funct. Mater.* **2012**, *22*, 5144−5156.
(22) Angelos, S.; Khashab, N. M.; Yang, Y. W.; Trabolsi, A.; Khatib, H. A.; Stoddart, J. F.; Zink, J. I. pH Clock-operated Mechanized Nanoparticles. *J. Am. Chem. Soc.* **2009**, *131*, 12912−12914.
(23) Wang, C.; Li, Z. X.; Cao, D.; Zhao, Y. L.; Gaines, J. W.; Bozdemir, O. A.; Ambrogi, M. W.; Frasconi, M.; Botros, Y. Y.; Zink, J. I.; Stoddart, J. F. Stimulated Release of Size-selected Cargos in Succession from Mesoporous Silica Nanoparticles. *Angew. Chem., Int. Ed.* **2012**, *51*, 5460−5465.
(24) Guillet-Nicolas, R.; Popat, A.; Bridot, J.; Monteith, G.; Qiao, S. Z.; Kleitz, F. pH-responsive Nutraceutical-mesoporous Silica Nanoconjugates with Enhanced Colloidal Stability. *Angew. Chem., Int. Ed.* **2013**, *52*, 2318−2322.
(25) Liu, R.; Zhang, Y.; Zhao, X.; Agarwal, A.; Mueller, L. J.; Feng, P. Y. pH-responsive Nanogated Ensemble Based on Gold-capped Mesoporous Silica through an Acid-labile Acetal Linker. *J. Am. Chem. Soc.* **2010**, *132*, 1500−1501.
(26) Lee, C. H.; Cheng, S. H.; Huang, I. P.; Souris, J. S.; Yang, C. S.; Mou, C. Y.; Lo, L. W. Intracellular pH-responsive Mesoporous Silica Nanoparticles for the Controlled Release of Anticancer Chemotherapeutics. *Angew. Chem., Int. Ed.* **2010**, *49*, 8214−8219.
(27) Gan, Q.; Lu, X.; Yuan, Y.; Qian, J.; Zhou, H.; Lu, X.; Shi, J.; Liu, C. A Magnetic, Reversible pH-responsive Nanogated Ensemble Based on Fe_3O_4 Nanoparticles-capped Mesoporous Silica. *Biomaterials* **2011**, *32*, 1932−1942.
(28) Li, L.; Tang, F.; Liu, H.; Liu, T.; Hao, N.; Chen, D.; Teng, X.; He, J. *In Vivo* Delivery of Silica Nanorattle Encapsulated Docetaxel for Liver Cancer Therapy with Low Toxicity and High Efficacy. *ACS Nano* **2010**, *4*, 6874−6882.
(29) Feng, W.; Zhou, X. J.; He, C. L.; Qiu, K. X.; Nie, W.; Chen, L.; Wang, H. S.; Mo, X. M.; Zhang, Y. Z. Polyelectrolyte Multilayer Functionalized Mesoporous Silica Nanoparticles for pH-responsive Drug Delivery: Layer Thickness-dependent Release Profiles and Biocompatibility. *J. Mater. Chem. B* **2013**, *1*, 5886−5898.
(30) Luo, Z.; Cai, K. Y.; Hu, Y.; Zhao, L.; Liu, P.; Duan, L.; Yang, W. H. Mesoporous Silica Nanoparticles End-capped with Collagen: Redox-responsive Nanoreservoirs for Targeted Drug Delivery. *Angew. Chem., Int. Ed.* **2011**, *50*, 640−643.
(31) Moon, D. S.; Lee, J. K. Tunable Synthesis of Hierarchical Mesoporous Silica Nanoparticles with Radial Wrinkle Structure. *Langmuir* **2012**, *28*, 12341−12347.
(32) Huang, Y. R.; He, S.; Cao, W. P.; Cai, K. Y.; Liang, X. J. Biomedical Nanomaterials for Imaging-guided Cancer Therapy. *Nanoscale.* **2012**, *4*, 6135−6149.
(33) Chen, Q.; Wang, C.; Zhan, Z. X.; He, W. W.; Cheng, Z. P.; Li, Y. Y.; Liu, Z. Near-infrared Dye Bound Albumin with Separated Imaging and Therapy Wavelength Channels for Imaging-guided Photothermal Therapy. *Biomaterials* **2014**, *35*, 8206−8214.
(34) Ali, Z.; Abbasi, A. Z.; Zhang, F.; Arosio, P.; Lascialfari, A.; Casula, M. F.; Wenk, A.; Kreyling, W.; Plapper, R.; Seidel, M.; Niessner, R.; Knöll, J.; Seubert, A.; Parak, W. J. Multifunctional Nanoparticles for Dual Imaging. *Anal. Chem.* **2011**, *83*, 2877−2882.
(35) Rivera_Gila, P.; Yang, F.; Thomas, H.; Li, L.; Terfort, A.; Parak, W. J. Development of an Assay Based on Cell Counting with Quantum Dot Labels for Comparing Cell Adhesion within Cocultures. *Nano Taday* **2011**, *6*, 20−27.
(36) Jo, C.; Lee, H. J.; Oh, M. H. One-Pot Synthesis of Silica@ Coordination Polymer Core-shell Microspheres with Controlled Shell Thickness. *Adv. Mater.* **2011**, *23*, 1716−1719.
(37) Hermes, S.; Schröder, F.; Chelmowski, R.; Wöll, C.; Fischer, R. A. Selective Nucleation and Growth of Metal-organic Open Framework Thin Films on Patterned $COOH/CF_3$-terminated Self-assembled Monolayers on Au (111). *J. Am. Chem. Soc.* **2005**, *127*, 13744−13745.
(38) Kreno, L. E.; Hupp, J. T.; Duyne, R. P. V. Metal-organic Framework Thin Film for Enhanced Localized Surface Plasmon Resonance Gas Sensing. *Anal. Chem.* **2010**, *82*, 8042−8046.
(39) Cai, K. Y.; Hu, Y.; Luo, Z.; Kong, T.; Lai, M.; Sui, X. J.; Wang, Y. L.; Yang, L.; Deng, L. H. Cell-specific Gene Transfection from a Gene-functionalized Poly(d,l-lactic acid) Substrate Fabricated by the Layer-by-Layer Assembly Technique. *Angew. Chem., Int. Ed.* **2008**, *47*, 7479−7481.
(40) Aina, O. H.; Sroka, T. C.; Chen, M. L.; Lam, K. S. Therapeutic Cancer Targeting Peptides. *Pept. Sci.* **2002**, *66*, 184−199.
(41) Li, Z. Y.; Liu, Y.; Hu, J. J.; Xu, Q.; Liu, L. H.; Jia, H. Z.; Chen, W. H.; Lei, Q.; Rong, L.; Zhang, X. Z. Stepwise-Acid-Active Multifunctional Mesoporous Silica Nanoparticles for Tumor-Specific Nucleus-Targeted Drug Delivery. *ACS Appl. Mater. Interfaces* **2014**, *6*, 14568−14575.
(42) Ma, X.; Zhao, Y.; Ng, K. W.; Zhao, Y. L. Integrated Hollow Mesoporous Silica Nanoparticles for Target Drug/siRNA Co-Delivery. *Chem.—Eur. J.* **2013**, *19*, 15593−15603.
(43) Sudimack, J.; Lee, R. J. Targeted Drug Delivery via the Folate Receptor. *Adv. Drug Delivery Rev.* **2000**, *41*, 147−162.
(44) Du, X.; He, J. H. Fine-Tuning of Silica Nanosphere Structure by Simple Regulation of the Volume Ratio of Cosolvents. *Langmuir* **2010**, *26*, 10057−10062.
(45) Li, M.; Zhang, C.; Yang, X. L.; Xu, H. B. Microfluidization-assisted Synthesis of Hollow Mesoporous Silica Nanoparticles. *J. Sol-Gel Sci. Technol.* **2013**, *67*, 501−506.
(46) Muhammad, F.; Guo, M.; Qi, W.; Sun, F.; Wang, A.; Guo, Y.; Zhu, G. pH-triggered Controlled Drug Release from Mesoporous Silica Nanoparticles via Intracelluar Dissolution of ZnO Nanolids. *J. Am. Chem. Soc.* **2011**, *133*, 8778−8781.
(47) Xu, S.; Liu, J.; Li, D.; Wang, L. M.; Guo, J.; Wang, C. C.; Chen, C. Y. Fe-salphen Complexes from Intracellular pH-triggered Degradation of Fe_3O_4@Salphen-InIII CPPs for Selectively Killing Cancer Cells. *Biomaterials* **2014**, *35*, 1676−1685.
(48) Cai, K. Y.; Hou, Y. H.; Hu, Y.; Zhao, L.; Luo, Z.; Shi, Y. S.; Lai, M.; Yang, W. H.; Liu, P. Correlation of the Cytotoxicity of TiO_2 Nanoparticles with Different Particle Sizes on a Sub-200-nm Scale. *Small* **2011**, *7*, 3026−3031.
(49) Saul, J. M.; Annapragada, A.; Natarajan, J. V.; Bellamkonda, R. V. Controlled Targeting of Liposomal Doxorubicin via the Folate Receptor *in vitro*. *J. Controlled Release* **2003**, *1*−*2*, 49−67.
(50) Iwasa, A.; Akita, H.; Khalil, I.; Kogure, K.; Futaki, S.; Harashima, H. Cellular Uptake and Subsequent Intracellular Trafficking of R8-liposomes Introduced at Low Temperature. *Biophys. Acta.* **2006**, *1758*, 713−720.
(51) Iversena, T.; Skotlanda, T.; Sandvig, K. Endocytosis and Entracellular Transport of Nanoparticles: Present Knowledge and Need for Future Studies. *Nano Today* **2011**, *6*, 176−185.
(52) Koivusalo, M.; Welch, C.; Hayashi, H.; Scott, C. C.; Kim, M.; Alexander, T.; Touret, N.; Hahn, K. M.; Grinstein, S. Amiloride Inhibits Macropinocytosis by Lowering Submembranous pH and Preventing Rac1 and Cdc42 Signaling. *J. Cell. Biol.* **2010**, *188*, 547−563.
(53) Meng, H.; Yang, S.; Li, Z.; Xia, T.; Chen, J.; Ji, Z.; Zhang, H.; Wang, X.; Lin, S.; Huang, C.; Zhou, Z. H.; Zink, J. I.; Nel, A. E. Aspect Ratio Determines the quantity of Mesoporous Silica Nanoparticle Uptake by a Small GTPase-dependent Macropinocytosis Mechanism. *ACS Nano* **2011**, *6*, 4434−4447.
(54) Suen, W.-L. L.; Chau, Y. Size-dependent Internalisation of Folate-decorated Nanoparticles via the Pathways of Clathrin and Caveolae-mediated Endocytosis in ARPE-19 Cells. *J. Pharm. Pharmacol.* **2014**, *66*, 564−573.
(55) Luo, Z.; Cai, K. Y.; Hu, Y.; Li, J. H.; Ding, X. W.; Zhang, B. L.; Xu, D. W.; Yang, W. H.; Liu, P. Redox-responsive Molecular Nanoreservoirs for Controlled Intracellular Anticancer Drug Delivery Based On Magnetic Nanoparticle. *Adv. Mater.* **2012**, *24*, 431−435.

DOI: 10.1021/acsami.5b00746
ACS Appl. Mater. Interfaces 2015, 7, 7357−7372

(56) Wang, F.; Wang, Y. C.; Dou, S.; Xiong, M. H.; Sun, T. M.; Wang, J. Doxorubicin-tethered Responsive Gold Nanoparticles Facilitate Intracellular Drug Delivery for Overcoming Multidrug Resistance in Cancer Cells. *ACS Nano* **2011**, *5*, 3679−3692.
(57) Dhar, S.; Kolishetti, N.; Lippard, J. S.; Farokhzad, C. O. Targeted Delivery of a Cisplatin Prodrug for Safer and More Effective Prostate Cancer Therapy *in Vivo*. *Proc. Natl. Acad. Sci. U.S.A.* **2011**, *108*, 1850−1855.
(58) Meng, H.; Mai, X. W.; Zhang, H.; Xue, M.; Xia, T.; Lin, S.; Wang, X.; Zhao, Y.; Ji, Z. X.; Zink, J. F.; Nel, A. E. Codelivery of an Optimal Drug/siRNA Combination using Mesoporous Silica Nanoparticles to Overcome Drug Resistance in Breast Cancer *in Vitro* and *in Vivo*. *ACS Nano* **2013**, *7*, 994−1005.
(59) Yang, K.; Xu, H.; Cheng, L.; Sun, Y. C.; Wang, J.; Liu, Z. *In Vitro* and *in Vivo* Near-Infrared Photothermal Therapy of Cancer Using Polypyrrole Organic Nanoparticles. *Adv. Mater.* **2012**, *24*, 5586−5592.
(60) Zheng, Y.; Liu, Y.; Jin, H.; Pan, S.; Qian, Y.; Huang, C.; Zeng, Y.; Luo, Q.; Zeng, M.; Zhang, Z. Scavenger Receptor B1 is a Potential Biomarker of Human Nasopharyngeal Carcinoma and Its Growth is Inhibited by HDL-mimetic Nanoparticles. *Theranostics* **2013**, *3*, 477−486.
(61) Yang, M.; Chen, J.; Cao, W. G.; Ding, L. L.; Ng, K. K.; Jin, H. L.; Zhang, Z. H.; Zheng, G. Attenuation of Nontargeted Cell-kill using a High-Density Lipoprotein-mimicking Peptide Phospholipid Nanoscaffold. *Nanomedicine* **2011**, *6*, 631−641.
(62) Maeda, H.; Wu, J.; Sawa, T.; Matsumurab, Y.; Hori, K. Tumor Vascular Permeability and the EPR Effect in Macromolecular Therapeutics: a Review. *J. Controlled Release* **2000**, *65*, 271−284.
(63) Park, J. H.; Gu, Luo.; Maltzahn, G. V.; Ruoslahti, E.; Bhatia, S. N.; Sailor, M. J. Biodegradable Luminescent Porous Silicon Nanoparticles for *in vivo* Applications. *Nat. Mater.* **2009**, *4*, 331−336.
(64) Kitaura, R.; Onoyama, G.; Sakamoto, H.; Matsuda, R.; Noro, S.-I.; Kitagawa, S. Immobilization of a Metallo Schiff Base into a Microporous Coordination Polymer. *Adv. Mater.* **2004**, *43*, 2684−2687.
(65) Wang, J.; Gao, P. P.; Yang, X. X.; Wang, T. T.; Wang, J.; Huang, C. Z. Real-time Imaging of Intracellular Drug Release from Mesoporous Silica Nanoparticles Based on Fluorescence Resonance Energy Transfer. *J. Mater. Chem. B* **2014**, *2*, 4379−4386.

DOI: 10.1021/acsami.5b00746
ACS Appl. Mater. Interfaces 2015, 7, 7357−7372